Spontaneous surface-induced long-range order in $Ga_{0.5}In_{0.5}P$ alloys

James E. Bernard, S. Froyen, and Alex Zunger
Solar Energy Research Institute, Golden, Colorado 80401
(Received 25 April 1991)

Previous total-energy calculations for bulk $Ga_{0.5}In_{0.5}P$ alloys have demonstrated that the lowest-energy configuration at $T=0$ corresponds to phase separation into GaP+InP, followed by the ordered $GaInP_2$ chalcopyrite phase as the next lowest state; the (111)-ordered CuPt-like superstructure is predicted to lie at a much higher energy. Yet, vapor-phase crystal growth has shown CuPt-like long-range ordering in relatively thick $Ga_{0.5}In_{0.5}P$ films grown on a lattice-matched (001) GaAs substrate. We present here first-principles local-density total-energy calculations for $Ga_{0.5}In_{0.5}P$/GaAs(001) in various two-dimensional structures, each having a free surface. For one-monolayer coverage, we find electronically driven surface reconstructions, consisting not only of the previously known cation dimerization, but also of buckling and tilting of the surface dimers. These considerably stabilize the CuPt-like surface topology over all other forms of surface order, including phase separation. Furthermore, a Ga/In layer covered by three monolayers still exhibits a significant energy preference (relative to kT_g, where $T_g \simeq 900$ K is the growth temperature) for the CuPt structure. If complete atomic mobility were to exist irrespective of how deeply buried the atoms are, we would then expect that the surface-stable CuPt ordering would exist in the near-surface regions, whereas deeper layers would revert to the bulk-stable structures. Since, however, surface atomic mobilities are far larger than bulk mobilities, it is possible that surface-stabilized structures will be frozen in and consequently ordering will propagate into macroscopic film dimensions. In light of our results, we describe several possible ways that surface effects could lead to long-range CuPt-like ordering.

I. INTRODUCTION: CAN ORDERED INTERSEMICONDUCTOR BULK COMPOUNDS BE STABLE?

Isovalent pseudobinary semiconductor alloys $A_{1-x}B_xC$ are widely used in electronic devices,[1,2] principally because they allow a continuous range of materials parameters, tunable by changing the composition x. Their utility in such applications rests largely on the possibility of achieving a single, *homogeneous* solid phase. Thermodynamically, however, such disordered single-phase bulk alloys are expected to be stable only at relatively high temperatures.[3-7] This can be seen by considering the excess enthalpy $\Delta H^{(\alpha)}_{\rm bulk}$ of phase α in bulk form defined as the energy of α with respect to the energy of equivalent amounts of the constituents AC and BC at their bulk equilibrium lattice parameters a_{AC} and a_{BC}:

$$\Delta H^{(\alpha)}_{\rm bulk} = E(\alpha, a_\alpha) - (1-x)E(AC, a_{AC}) - xE(BC, a_{BC}) . \quad (1)$$

Fitting the measured liquidus and solidus curves has shown[3,4] that *all* isovalent III-V and II-VI semiconductor alloys have $\Delta H^{(D)}_{\rm bulk} > 0$ for the α=disordered (D) phase. Hence such disordered alloys are expected to be thermodynamically stable only above a "miscibility gap" (MG) temperature $T_{\rm MG}$, where the negative entropy term $-T_{\rm MG}\Delta S$ overwhelms $\Delta H^{(D)}_{\rm bulk}$. Classic theories[3-7] explained why $\Delta H^{(D)}_{\rm bulk} > 0$ by postulating that all AC-BC interactions in such systems are fundamentally repulsive, due to the increase in elastic energy upon mixing constituents of dissimilar atomic sizes. Since the present paper deals with a *surface*-induced mechanism for ordering in III-V alloys, we first summarize in this section the current understanding of *bulk* ordering mechanisms, so that the need for alternative mechanisms becomes apparent.

First-principles total-energy calculations[8-17] have shown that $\Delta H^{(\alpha)}_{\rm bulk}$ consists of three contributions.

(i) A non-negative energy term associated with volume deformation of the constituents into the alloy's volume. This *volume-deformation* energy vanishes for size-matched binary components (e.g., AlAs-GaAs and CdTe-HgTe); otherwise, it scales with $(\Delta a)^2$, as correctly surmised by the classic elastic models.[3-7] This term tends to drive phase separation for alloys with $\Delta a \neq 0$.

(ii) A *strain-relief* term reflecting energy-lowering atomic relaxations that reduce the strain associated with packing different bond arrangements onto a fixed lattice.[10,14,17] Like the volume-deformation energy, this term is small for nearly size-matched components, but unlike it, the strain-relief term depends sensitively on the interfacial symmetry of the atomic arrangements. Among the *pseudobinary* adamantine $A_{1-x}B_xC$ systems, the chalcopyrite structure (Fig. 1) is best able to accommodate dissimilar tetrahedral arrangements,[14] whereas among *binary* adamantine $A_{1-x}B_x$ phases, the zinc-blende and the rhombohedral[18] RH1 structures have the lowest (in fact, zero) strain energies. Since the random alloy manifests a statistical distribution of (both stable and unstable) local atomic arrangements,[8] it is overall less able to accommodate strain than these special ordered structures. Strain relief can therefore drive selective or-

dering of the random alloy: for certain strain-minimizing ordered structures O one can have $\Delta H^{(O)}_{\rm bulk} < \Delta H^{(D)}_{\rm bulk}$ regardless of the sign of the two individual formation enthalpies.[9] The sum of the volume-deformation and strain-relief energies (total strain) can be zero only in topologically unconstrained[11] binary structures (e.g., zinc blende and RH1), which possess sufficient structural degrees of freedom to accommodate all of the bonding constraints. All pseudobinary adamantine structures are constrained, so for $\Delta a \neq 0$ their total strain energy is positive.[14]

(iii) The *charge-exchange* energy reflects chemical interactions attendant, e.g., upon charge transfer between the constituents.[10,15–17] For size-matched systems this can be conveniently modeled by the Madelung energy of a fixed lattice,[15] showing that among pseudobinary adamantine structures this term is lowest for the $AC+BC$ (phase-separated) system, followed by the (111)-oriented $(AC)_p(BC)_q$ superlattices and the random alloy. For size-mismatched systems, charge, in general, is transferred from the constituent with the smaller to that with the larger lattice constant.[10] This lowers the energy[10] if the direction of charge flow is toward the constituent with the larger electronegativity, i.e., if the smaller of the two constituents has the smaller electronegativity.

The results of quantitative first-principles total-energy calculations for a number of IV-IV, III-V, and II-VI intersemiconductor compounds in various structures[10–17] can be summarized in light of the above analysis, thus addressing the question posed in the title of this section, as follows.

(i) In size-*matched pseudobinary* systems (e.g., AlAs-GaAs or CdTe-HgTe), the constituent-strain and strain-relief energies vanish separately for all structures. Hence, the stability order is determined by the short-range chemical interactions, which are weakly repulsive. The lowest energy then corresponds to phase separation, followed by the (111) superstructures and by the random alloys as the next lowest energy phases. We hence do not expect, on the basis of thermodynamics, any ordered bulk intersemiconductor compounds in this class of materials.

(ii) In size-*mismatched binary* systems there are two cases. First, in $Si_{1-x}Ge_x$ the stability sequence is phase separation, followed by the random alloy, then the rhombohedral RH1 structure. Here, phase separation into Si+Ge is favored both by vanishing strain and charge-exchange energies, both of which are positive in the combined SiGe system. The "topologically unconstrained" RH1 (Ref. 18) and zinc-blende structures have vanishing total strain energies but unfavorable charge-exchange energies. The second case is exemplified by SiC. Like SiGe, SiC too has vanishing total strain energy in the topologically unconstrained structures.[11] However, strong charge transfer stabilizes its ordered phases (e.g., zinc-blende and its polytypes) over phase separation.[11] Hence, there are stable compounds for bulk SiC but not for SiGe.

(iii) In size-*mismatched pseudobinary* systems, such as $Ga_{1-x}In_xP$ or $GaAs_{1-x}Sb_x$, the stability sequence is phase separation, followed by the chalcopyrite structure and the random alloy; the (111) superstructures (Fig. 1) have the highest energies in this sequence. Again, phase separation is favored by vanishing strain and charge-exchange energies, while chalcopyrite is favored over the remaining structures by the favorable strain-relief energy. In the special case of the chalcopyrite phases of $AlInP_2$ and $AlInAs_2$, a combination of favorable strain relief and significant charge transfer from the smaller Al atom to the larger and more electronegative In atom leads to the prediction[10] that the CH phase of these two compounds is *absolutely* stable, so $\Delta H^{(\rm CH)}_{\rm bulk} < 0$. Hence, size-mismatched pseudobinary semiconductors are characterized by *metastable* chalcopyrite bulk ordering for all but $AlInP_2$ and $AlInAs_2$ for which *stable* chalcopyrite bulk ordering is predicted; all other ordered structures of this class are expected to be unstable.

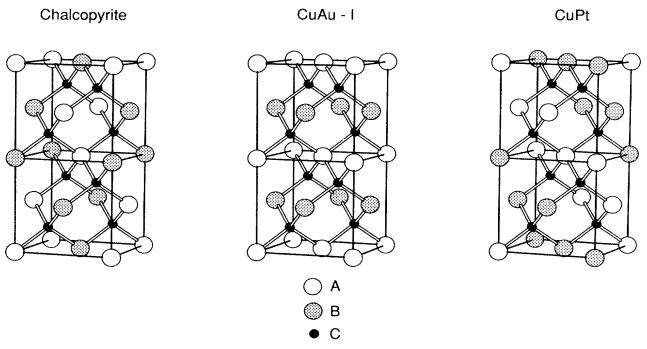

FIG. 1. Some of the observed ordered 3D structures of adamantine pseudobinary ABC_2 semiconductors.

II. INTERSEMICONDUCTOR COMPOUNDS IN THIN FILMS

All of the above expectations correspond to *bulk equilibrium* conditions appropriate to cases where the growing alloy is free to attain its three-dimensional minimum-energy crystal arrangement.[19] Vapor-phase crystal growth techniques such as organometallic vapor-phase epitaxy (OMVPE) or molecular-beam epitaxy (MBE) involve *thin* three-dimensional films that are often grown coherently on a fixed substrate. Recently, such OMVPE and MBE growth experiments have revealed spontaneous long-range order in a number of isovalent pseudobinary[20–39] and binary[40–43] semiconductor alloys. These ordered structures (see Fig. 1) can be described as short-period superlattices $(AC)_p(BC)_q$ whose atomic layers are oriented in the direction **G** (not necessarily the growth direction). The CuAu-I-like structure (CA) has $p=q=1$ and **G**=[001], the chalcopyrite (CH) structure has $p=q=2$ and **G**=[201] and the CuPt-like (CP) structure has $p=q=1$ and **G**=[111]. Observations of CA ordering in $AlGaAs_2/GaAs$ (110) were reported in Ref. 20, while CH ordering in $InGaAs_2/InP$ (110) was described in Ref. 31. A similar CH ordering was seen in Ga_2AsSb/InP (100) in Ref. 32, while the same material was reported also to order in the CP structure in Ref. 33. Indeed, CuPt ordering seems to be the most prevalent form: It has been seen also in $In_2AsSb/InSb$ (100),[34]

$AlInP_2/GaAs$ (100),[35] $GaInAs_2/InP$ (100) and GaInAsP,[36] $InAlAs_2/InP$ (100),[37] Ga_2AsP on a (100) alloy substrate[38] and AlGaInP/GaAs (100).[39] Rhombohedral-type ordering was seen in[40–43] $Si_{1-x}Ge_x$.

The prototype examples for ordering in pseudobinary $A_{1-x}B_xC$ alloys that we wish to discuss here are the CP ordering of $GaInP_2/GaAs$ (100) and the CA ordering of $AlGaAs_2/GaAs$ (110). Our foregoing discussion on the stability of various bulk intersemiconductor phases serves to explain why these particular forms of spontaneous long-range order are especially interesting.

(i) These isovalent alloys are known[3,4] to have positive mixing enthalpies $\Delta H^{(D)}_{\rm bulk} > 0$ when disordered, so ordered phases can represent stable equilibrium only in the unusual case[9] where special structures O have $\Delta H^{(O)}_{\rm bulk} < 0$ despite $\Delta H^{(D)}_{\rm bulk} > 0$. Initially, a number of calculations on $AlGaAs_2$ indicated that $\Delta H^{(\rm CA)}_{\rm bulk} < 0$ for the observed[20] CA structure. However, these were later shown[44–47] to be either incomplete or incorrect, so that in fact $\Delta H^{(\rm CA)}_{\rm bulk} > 0$ (actually, even[15,48] $\Delta H^{(\rm CA)} > \Delta H^{(D)}$ is true). Calculations on $GaInP_2$ also show[10] that $\Delta H^{(\rm CP)}_{\rm bulk} > \Delta H^{(D)}_{\rm bulk} > 0$. Hence, the observed ordering cannot represent bulk equilibrium.

(ii) Even if phase separation were slowed down by bulk kinetic limitations, calculations of $\Delta H^{(\alpha)}_{\rm bulk}$ and our foregoing discussions show that the next lowest-energy state of size-mismatched alloys is the chalcopyrite structure (observed[32] in $GaAs_{0.5}Sb_{0.5}$), not the CP structure seen in $GaInP_2$, whereas for the lattice-matched $Al_{0.5}Ga_{0.5}As$ alloy, the next states are the (111)-ordered structures and the random alloy, not the (100)-ordered CA structure. Therefore, even if the ordering were *metastable* (in the sense that an excited configuration is grown, then "frozen") bulk energetics indicates that this would not result in the structures that are actually observed for $Ga_{0.5}In_{0.5}P$ and $Al_{0.5}Ga_{0.5}As$.

(iii) In the case of lattice-mismatched systems, coherent epitaxial growth could stabilize the homogeneous phase by raising the energies of the *constituents*.[49] Here, one considers the case where the growing film is sufficiently thin so that the homogeneous phase α, as well as its decomposition products AC and BC, are all coherently matched in the parallel direction $a_\parallel$ to the substrate's lattice constant a_s (all other structural parameters relax subject to this constraint). In this case the relevant excess enthalpy[11(a)] is not that given by Eq. (1) but rather the energy relative to constituents that are *strained coherently:*

$$\Delta H^{(\alpha)}_{\rm epi} = E(\alpha, a_\parallel = a_s) - (1-x)E(AC, a_\parallel = a_s) - xE(BC, a_\parallel = a_s) \ . \quad (2)$$

Note therefore that if a_s is chosen to match the bulk equilibrium lattice constant of the homogeneous phase α (but $a_{AC} \neq a_{BC} \neq a_\alpha$), the existence of a substrate poses no effect on α but *raises* the energies of AC and BC. This could then expose the previously unstable ($\Delta H^{(\alpha)}_{\rm bulk} > 0$) homogeneous phase α as epitaxially stable, i.e., $\Delta H^{(\alpha)}_{\rm epi} < 0$. Calculations[49] have shown that such epitaxial-stabilization effects can suppress the bulk miscibility-gap temperature (indeed, the bulk-insoluble GaP-GaSb system has been observed[50] to exhibit extended solubility when grown epitaxially). However, such coherent epitaxial effects do not alter the *relative* stabilities[14] of the CH, the disordered, and the CP phases of $Ga_{0.5}In_{0.5}P/GaAs$. For the lattice-matched $Al_{0.5}Ga_{0.5}As/GaAs$ system coherent epitaxy has no effect since $a_{AC} \cong a_{BC} \cong a_s$.

Hence, our current theoretical understanding suggests that neither bulk thermodynamics nor coherent epitaxial effects can explain the ordered CP structure seen in $GaInP_2$ or the CA structure seen in $AlGaAs_2$. Such observations are nevertheless of great practical interest, as the optical properties of such "ordered alloys" are substantially different from those of the disordered alloys of the same composition.[24] This opens the possibility of tuning alloy properties (through selection of growth parameters controlling ordering) even at fixed composition. Before abandoning a thermodynamic reasoning for ordering in favor of some "kinetic factors," we examine next the role that *surface energetics* might play.

III. THE POSSIBILITY OF SURFACE-INDUCED INTERSEMICONDUCTOR ORDERED COMPOUNDS

There are experimental indications[21,23,29,33] suggesting that the CP-type ordering could be induced at the free surface during growth. If the [111] ordering were of bulk origin one would expect all four {111} variants to be present (these are equivalent in the bulk by symmetry); only two, however (the $[1\bar{1}1]$ and $[\bar{1}11]$ denoted as CP_B; the other two are CP_A), are seen.[21,29,33] Furthermore, a given type of ordering is frequently observed only for growth on a given substrate orientation.[22] We will therefore consider the excess energies of various epitaxially coherent phases α, each having a *free surface:*

$$\Delta H^{(\alpha)}_{\rm surf} = E(\alpha_{\rm surf}, a_\parallel = a_s) - (1-x)E(AC_{\rm surf}, a_\parallel = a_s) - xE(BC_{\rm surf}, a_\parallel = a_s) \ . \quad (3)$$

Like in the three-dimensional (3D) structures underlying Eq. (2), here too, coherent epitaxy will tend to suppress phase separation. However, unlike the 3D case, the existence of a free surface permits both new, strain-relieving relaxations and electronically driven reconstructions. We will therefore investigate the possibility that the lowest-energy atomic topology *at the free surface* of an alloy is qualitatively different from that of the three-dimensional bulk. While surface structures without bulk counterparts often have been observed in metal alloys,[51] these persist only for a few monolayers. The far slower bulk diffusion in semiconductors could, however, cause the surface-*stable* topology to be retained *metastably* after the surface has been covered by growth of subsequent layers. This would lead to the unusual effect of surface-induced ordering that propagates to macroscopic length scales. We focus here on $Ga_{0.5}In_{0.5}P$ on the (001) GaAs substrate and contrast $\Delta H^{(\alpha)}_{\rm surf}$ for this alloy with the corresponding values for $Al_{0.5}Ga_{0.5}As$, which does not order on (001) substrates [it does[20] on the (110) surface, which is not considered here].

Previous theories[25,52,53] have considered elastically driven surface-*relaxation* (not reconstruction) effects as a possible driving force for ordering. We find (Sec. V), however, that the resulting energy differences between the various competing topologies are too small to account for ordering at a (typical) growth temperature (T_g) of 900 K. Another model[29] discussed ordering in terms of *ad hoc* "growth rules," which were designed to produce the observed CP structure but lack any other justification. We have performed first-principles total-energy calculations for P-terminated and Ga/In-terminated $GaInP_2$ bilayers on a GaAs substrate, permitting the cation layer to take up different topologies, ranging from phase separated to various ordered structures. The presence of such a free surface leads to surface reconstructions. Our calculations show that for the cation-terminated surface such *electronically driven surface reconstructions* (i.e., dimerization, buckling, and tilting, see Sec. V) *stabilize the observed CP_B structure of $GaInP_2$ (but not $AlGaAs_2$) over other structures by 84 meV per surface atom,* so this type of surface ordering is predicted to be thermodynamically preferred at T_g. We have next considered structural preferences for "buried" Ga/In layers. While coverage is certain to undo the reconstruction of buried layers, it is possible that the reconstruction of the *top* (surface) layer would exert (chemical or elastic) effects a few layers below the surface, thus stabilizing there a certain atomic "topology" over the others. In systems with buried Ga/In layers the Ga/In layers below the top two layers have a bulklike environment, so we use the computationally simpler valence-force-field (VFF) method[54] (whose parameters are fit to first-principles results) to calculate the relative stability of such "buried" layers. We consider various arrangements of 2, 4, or 6 monolayers (referring to each cation and anion layer as a monolayer) of GaInP on a GaAs substrate of at least 11 monolayers, with the deepest Ga/In layer denoted as the hth subsurface layer. The top two monolayers (surface $h=0$ and first subsurface $h=1$) are kept fixed at the geometry determined from first-principles calculations, with all remaining atomic positions being relaxed to minimize the VFF energy. *We find that CP_B is selectively stabilized also for $h=3$.* Our calculations hence show that surface reconstruction not only favors atomic arrangements that are unstable in the bulk, but that it also results in energy differences large enough to produce order at T_g. Of course, the chemical or elastic influence of the top surface can penetrate only a few layers into the film. Hence, even though we find that the CP_B structure is energetically preferred at the third subsurface layer, this structure would not propagate much deeper if atoms could diffuse freely inside the bulk (recall that the CH, not the CP structure is the stablest in bulk form). However, if atomic mobility decreases sufficiently rapidly below the growing surface, the CP_B structure formed at the surface would be frozen in and perpetuated throughout the film. In light of our results, we propose in Sec. VIII several possible scenarios by which the full three-dimensional CP_B structure could be formed near the surface and frozen in by subsequent growth. We next discuss the meaning of such constraints on atomic mobilities in deep layers.

IV. METHOD OF CALCULATION

A. Basic premises and approximations

Bulk thermodynamic models assume that sufficient atomic mobility exists during growth so that atoms can always explore and find their global equilibrium positions; the *microscopic structure* of the crystal then does not depend on the way it was grown. While this is often the case in melt and solution growth, low-temperature vapor growth techniques are characterized by large surface mobilities but by small mobilities for atoms in the solidified, buried layers. Our basic premise here will be that at the *free* surface, atoms will take up only energy-minimizing positions, but that when buried by subsequent layers the topology (but not the reconstruction) established at the free surface is frozen in, even though it no longer represents the lowest energy of the bulk. The term "topology" requires some explanation: we know[55,56] that, e.g., cation-terminated (001) surfaces of zinc-blende semiconductors exhibit dimerization and possibly other forms of reconstruction. For an alloy surface we need to distinguish between such structural degrees of freedom (which we denote as "geometry") and the overall surface pattern or connectivity of the alloy atoms (which we denote as "topology"). We hence assume that subsequent coverage of the surface freezes in the surface-stable topology (although coverage must, of course, undo surface-driven relaxation and dimerization). The *number* of adlayers h_c required to effectively halt atomic diffusion is unknown, and will be treated as a parameter. In bulk equilibrium $h_c \to \infty$.

If h_c is a *single* monolayer, one expects that the energy-minimizing Ga/In topology of the cation-terminated surface would be perpetuated during growth, since each new Ga/In layer would adopt this topology and each buried layer would be frozen in this topology. We will hence determine first the energy-minimizing structure of the cation-terminated surface (Sec. V). If h_c is larger, one expects that the structure and topology of the top layer could still influence the topology a few layers below, e.g., through subsurface strain.[57] Conversely, ordered buried layers could influence the placement of the surface reconstructions, an effect that could produce the correct layer phasing necessary to build up a true three-dimensional CP_B structure. We will therefore calculate next $\Delta H^{(\alpha)}_{\rm surf}$ for various Ga/In layers that are 1, 2, 3, 4, and 5 monolayers below the surface (Secs. VI and VII). Finally, if h_c is even larger, one expects to recover the result of three-dimensional epitaxial calculations.

The present approach differs from Monte Carlo growth-simulation models,[58,59] which explore the effect on the free surface of *kinetic* variables such as activation barriers for adsorption, migration, and desorption of individual atoms. Instead, we assume a complete (flat) surface and explore its *equilibrium* structure and energy. Our approach is also distinct from molecular dynamics

simulations,[60] which study the time evolution of the *kinetic pathway,* or from stochastic growth models,[61] which search for a set of empirical "growth rules" producing (through atomistic simulations) a desired atomic order without minimizing any energy functional. Hence, our basic approach consists of exploring first the extent to which surface equilibrium effects [through Eq. (3)] can explain ordering, falling back on kinetic arguments only when the former approach fails to explain the observations.

We describe the (001) surface structure of the alloy using a (2×2) surface unit cell. This cell is large enough to describe the topologies of several common bulk structures (including CP, CH, and CA) yet simple enough to be treated using the first-principles pseudopotential method. It differs from the observed[55] and calculated[56] (2×4) structure of GaAs (001), which is believed to be a partially covered surface.

There is evidence that surface steps are important for the selective growth of *one* of the two subvariants[22] of CP_B (either $[1\bar{1}1]$ or $[\bar{1}11]$) and may be responsible for periodic lateral phase separation observed, e.g., in[62] $Al_{1-x}Ga_xAs/GaAs$ (100). It has also been speculated that steps may be necessary for the correct CP_B stacking of the layers during growth. Our results show, however, that the CP_B structure can be achieved without the presence of steps, although step motion and other kinetic factors could determine the relative proportions of the two subvariants of CP_B.

B. Structure of supercells

The total excess energy $\Delta H^{(\alpha)}_{\rm surf}$ of Eq. (3) is calculated in a repeated slab geometry. Each structure has a few monolayers of GaAs representing the substrate and a few lattice-matched GaInP layers on top of it. Above them we retain a few empty layers; this structure is then repeated periodically. Our basic computational strategy is to compare the energies of such supercells, varying (i) the atomic topology of the Ga/In layer(s), and (ii) the depth h of the deepest Ga/In layer below the surface ($h=0$ denotes the surface layer). We hence fix the *topology* of the unit cell (i.e., the connectivity of atoms) but permit relaxations and reconstructions that lead to a minimum energy structure for each topology.

Considering first the energies of a *single* Ga/In surface layer on a (001) substrate we ask whether $\Delta H^{(\alpha)}_{\rm surf}$ of Eq. (3) can explain (i) the preference of ordering (CA, CP, CH) over phase separation in GaInP; (ii) the preference for CP over other structures (CA, CH, etc); (iii) the preference of CP_B over CP_A; and (iv) the absence of order in the lattice-matched $Al_{0.5}Ga_{0.5}As/GaAs$ (001) alloy. These questions can be phrased in terms of the relative stability of the five prototype (001) alloy bilayers shown in Fig. 2. By stacking these layers in different ways, several three-dimensional structures are obtained (Table I). These questions are addressed by calculating the appropriate $\Delta H^{(\alpha)}_{\rm surf}$ using the first-principles pseudopotential method.[63] Second, we ask whether an energetic preference persists between structures $a-e$ if such layers are buried h monolayers below the surface.

C. Pseudopotential calculations

Two types of slabs were used. The first, which was used for most of the cation-terminated surfaces, consisted of three atomic substrate layers (Ga-As-Ga) covered on each side by single, cation-terminated bilayers of $GaInP_2$ (or $AlGaAs_2$) in the topologies $a-e$ (of Fig. 2) and separated by four empty layers. The bottom and top layers are kept identical to prevent spurious charge transfer. The second type was a single-surface slab with a $Ga_{0.5}In_{0.5}P$ top surface and a GaAs bottom surface terminated by half a monolayer of Ga.[64] The bottom surface is semiconducting; this prevents spurious charge

TABLE I. 3D structures characterized by stacking of the (001) bilayers shown in Fig. 2. The structures are identified both by a superlattice notation (the direction **G** and the repeat period $2n$) and by the name used in the text. Each layer is shifted laterally as indicated in parentheses (in units of the zinc-blende lattice constant). Several other structures are degenerate with those tabulated: [110] $n=1$ is identical to [001] $n=1$ CA; [201] $n=2$ CH is degenerate with [021] $n=2$ CH, and [010] CA is degenerate with [100] CA. The [102] $n=2$ and [012] $n=2$ CH structures have (001) layers that cannot be represented by the 2×2 patterns in Fig. 2. Notice that the d layer occurs only in the observed CP_B phase and in the [110] $n=2$ superlattice. The two are distinguished only by the third layer stacking.

		Structure	Bilayer number			
G	n	Name	1	2	3	4
(binary)		A	$a(0,0)$	$a(\frac{1}{2},0)$	$a(0,0)$	$a(\frac{1}{2},0)$
(binary)		B	$b(0,0)$	$b(\frac{1}{2},0)$	$b(0,0)$	$b(\frac{1}{2},0)$
[021]	2	CH	$e(0,0)$	$e(\frac{1}{2},0)$	$e(\frac{1}{2},\frac{1}{2})$	$e(0,\frac{1}{2})$
[100]	1	CA	$e(0,0)$	$e(\frac{1}{2},0)$	$e(0,0)$	$e(\frac{1}{2},0)$
[001]	1	CA	$a(0,0)$	$b(\frac{1}{2},0)$	$a(0,0)$	$b(\frac{1}{2},0)$
[111]	1	CP_A	$c(0,0)$	$c(\frac{1}{2},0)$	$c(\frac{1}{2},\frac{1}{2})$	$c(0,-\frac{1}{2})$
[110]	2		$c(0,0)$	$c(\frac{1}{2},0)$	$c(0,0)$	$c(\frac{1}{2},0)$
$[\bar{1}11]$	1	CP_B	$d(0,0)$	$d(\frac{1}{2},0)$	$d(\frac{1}{2},-\frac{1}{2})$	$d(0,\frac{1}{2})$
$[\bar{1}10]$	2		$d(0,0)$	$d(\frac{1}{2},0)$	$d(0,0)$	$d(\frac{1}{2},0)$

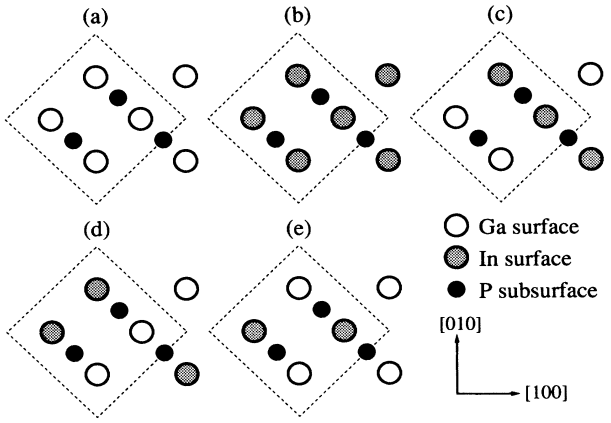

FIG. 2. Surface atomic arrangements for the 2×2 surface cell. See Table I for the description of the bulk structures that can be obtained by different stacking of these surface unit cells.

transfer between opposite surfaces. The single-surface slab is computationally more expensive but it allows relaxations five layers below the surface and was used to check our results. We use the first-principles local-density pseudopotential method[63] with the exchange correlation potential of Perdew and Zunger[65] to calculate the total energies of the slabs; quantum-mechanical forces[63] are used to find equilibrium geometries. In order to reduce the computational cost, we generated "soft" pseudopotentials using the method of Vanderbilt.[66] This allows us to achieve basis-set convergence with a relatively small plane-wave cutoff of only 10 Ry. The resulting lattice constants of the binary constituents (GaP, InP, GaAs, and AlAs) are about 4% smaller than experiment; the deviation, however, is uniform so lattice constant matches and/or mismatches are preserved. We use a 2D projection of the 10 face-centered-cubic special k points[67] to perform the surface Brillouin-zone integrals.

We have performed several tests in order to check that interactions between the two surfaces of our seven-layer slab did not bias our results (the geometry was separately relaxed in every case): (i) We added four additional layers of GaAs to the substrate and compared the unreconstructed surfaces $(a+b)$ and e. The energy difference changed by less than 3 meV per surface atom. (ii) For the fully relaxed geometries, we shifted the upper half of the slab by half the lattice constant of the surface unit cell. Energies changed by less than 6 meV. (iii) We fixed the atomic positions in the central layers of the slab in their ideal zinc-blende positions. Fixing one layer increased the energy of the e surface by 7 meV, and fixing three layers raised the energy by 17 meV. (iv) Finally, we compared our results from the normal slab, with those using a single-surface slab. The energy difference between the fully relaxed d and e surfaces changed by less than 4 meV. This last test allowed surface-induced relaxations to propagate five layers into the bulk. Based on these tests, we estimate that energy differences between the various surfaces are accurate to better than 10 meV per surface atom.

D. Valence-force-field calculations

Calculations for supercells representing thick (up to 17 monolayers) systems are done using the valence-force-field method. The total elastic energy of such supercell structures is minimized subject to the constraint that the top two $GaInP_2$ layers are fixed at the geometry found in self-consistent pseudopotential calculations. Hence, unlike Boguslawski,[52(a)] who used an unreconstructed surface, we explore here the energetic consequences of surface reconstruction on structural selectivity a few layers below the surface. We use as input to the VFF equilibrium bond lengths and elastic parameters determined directly from the pseudopotential calculations for zinc-blende GaP, InP, and GaAs and InAs. These differ somewhat from the empirical values tabulated, e.g., in Ref. 68. The structural optimization is carried out by directly relaxing the coordinates of the (nonfrozen) atoms using a conjugate-gradient method.[69] Since the top two monolayers are frozen in the pseudopotential-determined geometry, we omit from the energy calculation all bonds lying within those layers, as well as all bond angles involving exclusively atoms within those layers.

V. PSEUDOPOTENTIAL STUDIES OF THE CATION-TERMINATED SURFACES

A. Relative energies of various surface topologies of cation-terminated $GaInP_2$/GaAs (001)

1. Relaxed but unreconstructed surfaces

Calculated energies for relaxed but unreconstructed surfaces are given in the first row of Table II. In agreement with the calculations (but not the conclusions) of Boguslawski,[52(a)] all energy differences between unreconstructed surfaces (alloyed or phase separated) are considerably smaller than kT_g, where $T_g \sim 900$ K is the growth temperature. Similarly, the model of Matsumura, Kuwano, and Oki,[52(b)] which assumes an unreconstructed 1×1 surface unit cell, gives, in light of our calculated energies, the wrong ground-state structure and negligible order-disorder transition temperature. Clearly, surface effects without reconstruction do not give rise to any significant structural preference. Suzuki, Gomyo, and Iijima[25] suggested that surface-relaxation effects associated with incorporation of a large atom (In) create lateral strains that encourage subsequent acceptance of only a small atom (Ga) next to it. We find, however, that elastic size effects are more easily accommodated at the free surface (where atoms can relax freely in the perpendicular direction) than in the bulk, in that the energy differences indicated in the first line of Table II are smaller than those appropriate for the corresponding bulk systems (~40 meV/atom pair).[14] Hence, strain relief alone induces no structural preferences at the surface. Electronically we find that all unreconstructed surfaces are metals.

TABLE II. Surface energies for the varoius $GaInP_2/GaAs$ (001) reconstruction modes discussed in the text. The energies are in meV per surface atom relative to the unreconstructed $a+b$ (phase separated) surface (surfaces a and b have their own separate zero of energy). We show separately the results of the dimerzied+buckled+tilted (DBT) surface with Ga up and with In up.

Surface geometry	Surface type					
	a	b	$a+b$	c	d	e
Unreconstructed	0	0	0	14	−9	2
Dimerized	−785	−366	−575			−620
Dimerized+buckled	−732	−448	−590		−692	−602
DBT-Ga up	−836	−564	−701	−684	−623	−715
DBT-In up	−836	−564	−701	−684	−799	−705

2. *The reconstructed surface*

The situation changes significantly when reconstructions are permitted (Figs. 3 and 4). Surface dimerization results in heteropolar (Ga-In) dimers on surfaces c and e (Fig. 4) but in homopolar (Ga-Ga or In-In) dimers on surfaces a, b, and d (Fig. 3). Relative to the undimerized surfaces, dimerization lowers the energy by an average of 600 meV per surface atom (Table II, line 2).[70] In addition to dimerization we find in all cases two other energy-lowering reconstructions within the 2×2 surface unit cell. First, dimers relax perpendicularly to the surface creating $[\bar{1}10]$ dimer rows of alternating high and low dimers [e.g., see Fig. 4(c)]. We will refer to this as "buckling." This motion does not alter the symmetry of the d surface, where the two dimers are already distinct before

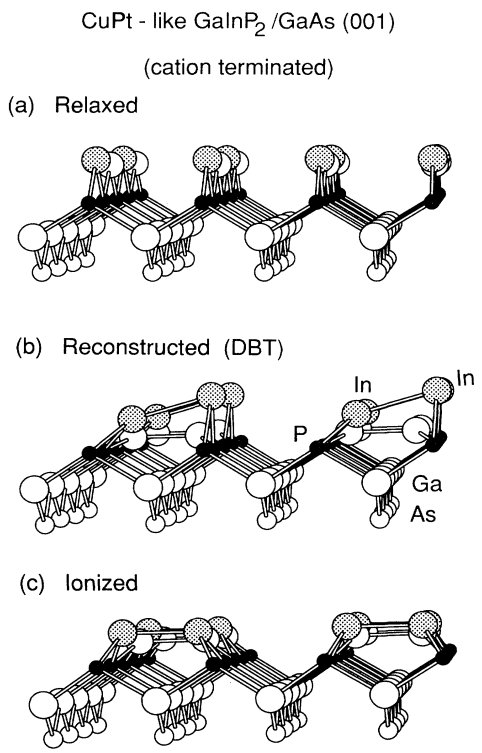

FIG. 3. Side view of atomic geometries for the cation terminated d (CP) surface of $GaInP_2$. The surface atoms are Ga (white), In (grey), and P (black) on top of a (001) substrate GaAs layer (white). (a) Relaxed but undimerized, (b) fully reconstructed with buckled and tilted dimers, and (c) ionized (Sec. V D).

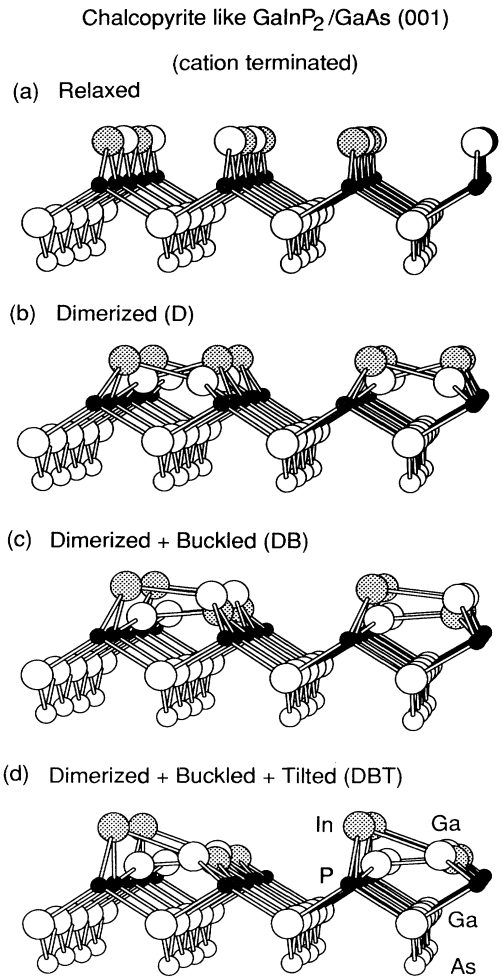

FIG. 4. Side view of atomic geometries for the various reconstruction modes described in the text for the cation terminated e (CH) surface of $GaInP_2$. The atoms for Ga (white), In (grey), and P (black) on top of a (001) substrate GaAs layer (white). (a) Relaxed but undimerized, (b) dimerized, (c) dimerized and buckled, and (d) fully reconstructed.

buckling, but it breaks the symmetry of the other surfaces. Buckling lowers the energy of the *b* surface (Table II, line 3), but raises the energy for surfaces *a* and *e* (so these surfaces will not buckle). Second the high dimer tilts in the [110] direction becoming nonhorizontal, whereas the low dimer remains virtually horizontal [e.g., see Fig. 4(d)]. This tilt is natural for surfaces with heteropolar dimers (*c* and *e*), but constitutes a symmetry breaking for the other surfaces [see Fig. 3(b)]. Since the four surface sites are inequivalent in the final geometry, there are two different ways of distributing the two Ga and the two In atoms in each of the topologies, *c*, *d*, and *e*. We will characterize this by the type of atom (Ga or In) occupying the site on the high dimer that tilts upwards. The third and fourth lines of Table II show that the *d* surface strongly prefers having the larger In atom on the high dimer, whereas the *c* and *e* surfaces show a slight preference for the smaller (but more electronegative) Ga atom to be tilted up. Tilting leads to a uniform energy lowering of 100 meV but does not affect the relative stability of the surfaces[71] (Table II, lines 3 and 4). This insensitivity of the relative surface energies to tilting of the high dimer suggests that the low dimer might be responsible for the increased stability of the *d* surface over the others. Note from Table I that among the $a+b$, *c*, *d*, and *e* surfaces, *d* is the only one where the low dimer contains only small atoms (Ga-Ga). Therefore, it is best able to relax into the electronically optimal (see below) geometry where it becomes nearly coplanar with the P atoms.

As shown in Table II, the reconstructions (dimerization, buckling, and tilting) considerably lower the energy of all the surfaces and, most significantly, make the surface corresponding to the observed CP_B ordering (*d*) the lowest in energy by 84 meV per surface atom. *Thus, surface reconstruction not only favors atomic arrangements that are unstable in the bulk, but it also results in energy differences large enough to produce order at* T_g.

Note that in $GaInP_2$/GaAs the CH surface *e* (observed[32] in Ga_2AsSb) is the next lowest-energy structure after CP_B and that the CP_A structure (never observed) is the highest-energy member in this series. Within the precision of our calculation we hence find that surface reconstruction of a cation layer changes the energy order $CH < CA \lesssim (a+b) < CP_A = CP_B$ found in the bulk,[10,14] yielding instead $CP_B \lesssim CH \lesssim (a+b) < CP_A$.

Ogale, Thomsen, and Madhukar[59] noted in their Monte Carlo simulation of the growth of (001) $Al_{0.33}Ga_{0.67}As$ that if one assumes some simple form of surface reconstruction this can produce ordering in the following adsorbed layer through modification of *kinetic* parameters. We have shown here that electronic effects at the surface can lead to a *thermodynamic* (as opposed to kinetic) preference for ordering. Kondow *et al.*[26] suggested that CP_B ordering in $GaInP_2$/GaAs (100) is kinetically driven, since at its growth temperature the bulk disordered alloy or phase separation should have been observed. However, it has been shown before[49,50] that coherence of a film with its substrate can remove phase separation from contention even without the presence of a surface or kinetic effects.

B. Electronic structure: A negative-*U* system

We find that all of the reconstructions in GaP, InP, and $GaInP_2$, are electronically driven. Unreconstructed cation surfaces have two broken bonds per surface atom, each containing $\frac{3}{4}$ electron. When two surface atoms dimerize, two of their three electrons occupy the bonding orbital [Figs. 5(c) and 5(d)]. This leaves one unpaired electron per dimer; hence the unbuckled, dimerized (2×2) surface is metallic. Energy can, however, be lowered by breaking the symmetry through buckling and tilting. Of the four atoms in a dimer pair, we find that three relax toward planar sp^2-like configurations and the fourth atom moves up into a pyramidal s^2p^3-like configuration with bond angles approximating 90°. This allows the fourth atom to bind the two unpaired electrons

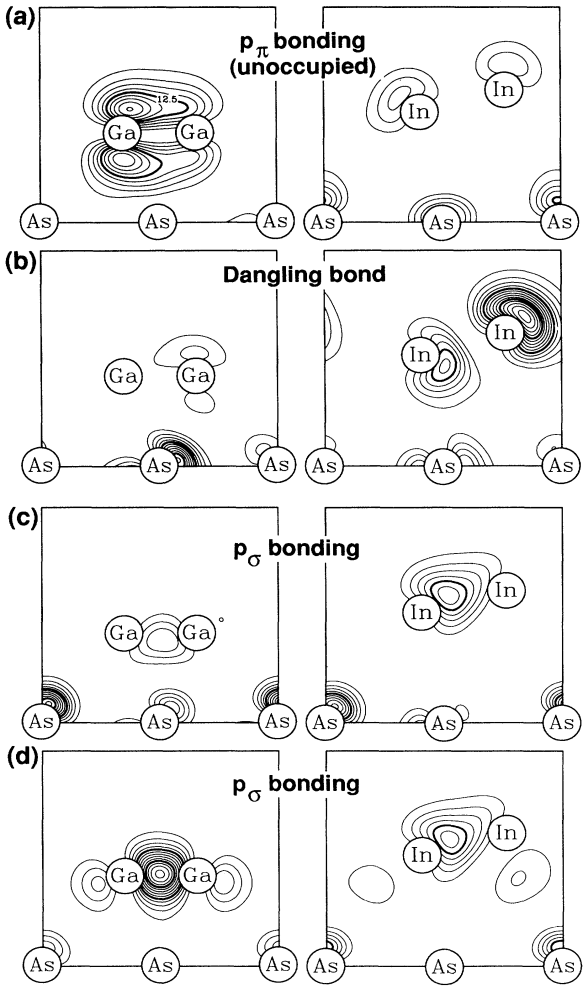

FIG. 5. Contour plots of selected surface states for the *d* surface at the Γ point in the Brillouin zone in two cuts (through the low Ga-Ga dimer, left, and the high In-In dimer, right). (a) shows a Ga-Ga p_π bonding state (lowest unoccupied state), (b) shows an In dangling-bond state (highest occupied state), and (c) and (d) show the deeper Ga-Ga and In-In p_σ bonding states.

in a "dangling-bond" (lone-pair) state [Fig. 5(b)]. Hence, the high atom acts as an "anion," receiving electrons from the low atoms that behave therefore as "cations." The lowest unoccupied state is a bonding p_π state on the low dimer [Fig. 5(a)]. Note therefore that a pair of dimers forms a negative-U system where two neutral (horizontal) dimers are unstable with respect to disproportionation into a positively charged low (L) dimer and a negatively charged high (H) dimer. For example,

$$(\mathrm{Ga}-\mathrm{Ga})^0+(\mathrm{In}-\mathrm{In})^0 \xrightarrow{U(\mathrm{CP}_B)} (\mathrm{Ga}-\mathrm{Ga})_L^+ + (\mathrm{In}-\mathrm{In})_H^- . \quad (4)$$

The energy gain involved (difference between the fifth and the second lines of Table II) is as large as $U=-200$ meV/surface atom.

C. Structure of relaxed and reconstructed $GaInP_2$ surfaces

Figures 6(a)–6(e) tabulate the geometries of fully relaxed and reconstructed cation surfaces for the neutral $GaInP_2$/GaAs (001) system. In addition to the bond-angle changes already discussed, several features are noteworthy: (i) The cation-anion bond lengths are mainly determined by the dimer type (high or low). The bond lengths for the high dimers are 6% and 11% longer than the bond lengths for the low dimer, whereas the difference between Ga-P and In-P bond lengths for a given dimer type is only 6%. (ii) The cation-cation dimer bond lengths are comparable to the cation-anion bond lengths and are longer for the high dimer and for dimers containing In. (iii) For a given dimer type (high or low), and occupation (by Ga or In) the geometry is highly transferable. For example, the low dimer on the a surface is almost identical to the low dimer on the d surface. Similarly, compare high b with high d and high c with high e. Even the low dimer on the c surface resembles the low dimer on the e surface after 180° rotation. (iv) The low dimer, preferring coplanar bonding arrangement with its P neighbors, moves downward and the P sublayer atoms relax towards the high dimers in order to facilitate this. Low dimers with two small Ga atoms are able to achieve a more optimal bonding arrangement than dimers containing In.

D. Structural consequences of ionizing the dangling bonds

The foregoing analysis suggests that if the two electrons in the dangling-bond state on the high dimer [Fig. 5(b)] could be removed, e.g., by heavy p doping or by excitation, both dimers would prefer planar sp^2-like arrangements and the energy advantage of the d surface should vanish. To examine this, we have performed a total energy minimization for the doubly ionized surfaces. This showed that the total energy difference between the d^* and e^* surfaces (we denote ionized structures by an asterisk) is indeed reduced from 84 to 1 meV per surface atom; hence, the In dangling-bond electrons are indeed responsible for the buckling of CP_B. A side view of the resulting d^* surface is shown in Fig. 3(c) and the dimer

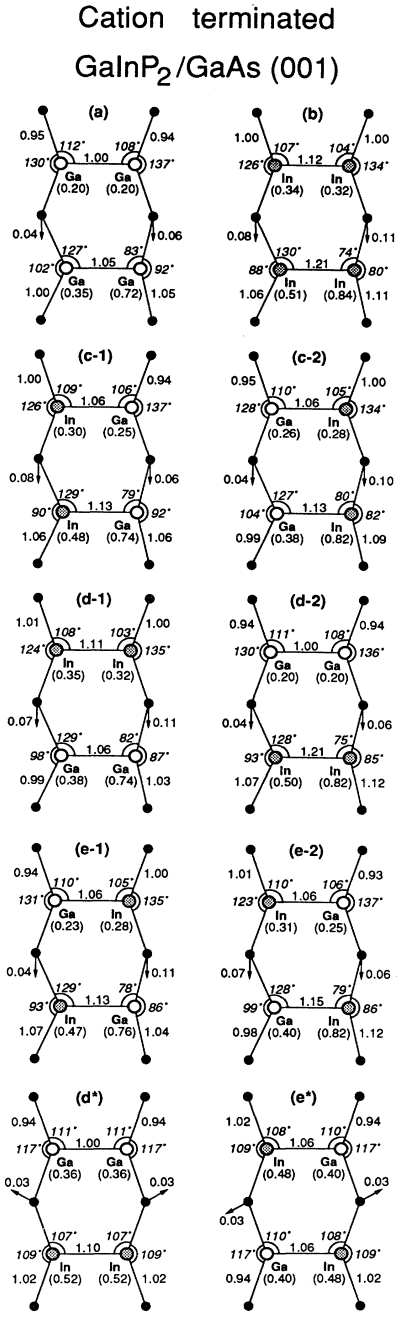

FIG. 6. Schematic top view of the 2×2 unit cell depicting fully relaxed and reconstructed geometries (dimerized, buckled, and tilted) of the five prototype cation-terminated $GaInP_2$ surfaces shown in Fig. 2. For the c, d, and e surfaces we show the two variants with Ga up (denoted 1) and In up (denoted 2). Parts (d*) and (e*) give the geometries for the ionized d and e surfaces. In addition to bond lengths and bond angles, the heights (in parentheses) of the Ga (white) and In (grey) atoms over the P (black) subsurface layer, and the approximate direction and magnitude of the horizontal displacement of the P atoms from their ideal zinc-blende positions are given. Individual vertical displacements of the P atoms are all small. Lengths are given in units of the average of the bond lengths of bulk GaP and InP. In these units, the bulk bond lengths of GaP and InP are 0.96 and 1.04, respectively.

geometries are tabulated in Fig. 6 [see (d*) and (e*)]. We would expect the ionized surfaces to have dimer geometries similar to the low dimer geometries for the neutral surfaces. Comparing the two, we see that the bond lengths are closely preserved but that dimers on the ionized surfaces sit higher above the P layer than the corresponding low dimers on the neutral surfaces. This is because the P atoms in the former case are unable to relax. The vanishing (d*) vs (e*) energy difference upon ionization is a possible explanation for the fact that *p*-doped samples show dramatically reduced ordering[23]; it also opens the possibility for undoing the reconstruction (hence, ordering) by optical excitations during growth. This argument also shows that ordering depends on coverage: if the cation surface coverage Θ is less than $\frac{3}{4}$ monolayer, all high dimer dangling-bond electrons can transfer to the P dangling bonds with a consequent loss of structural selectivity. For $\frac{3}{4} < \Theta < 1$ the transfer is partial. We therefore expect that the contribution to ordering from reconstructed cation surfaces will be reduced for surfaces with $\frac{3}{4} < \Theta < 1$ and vanish for $\Theta < \frac{3}{4}$.

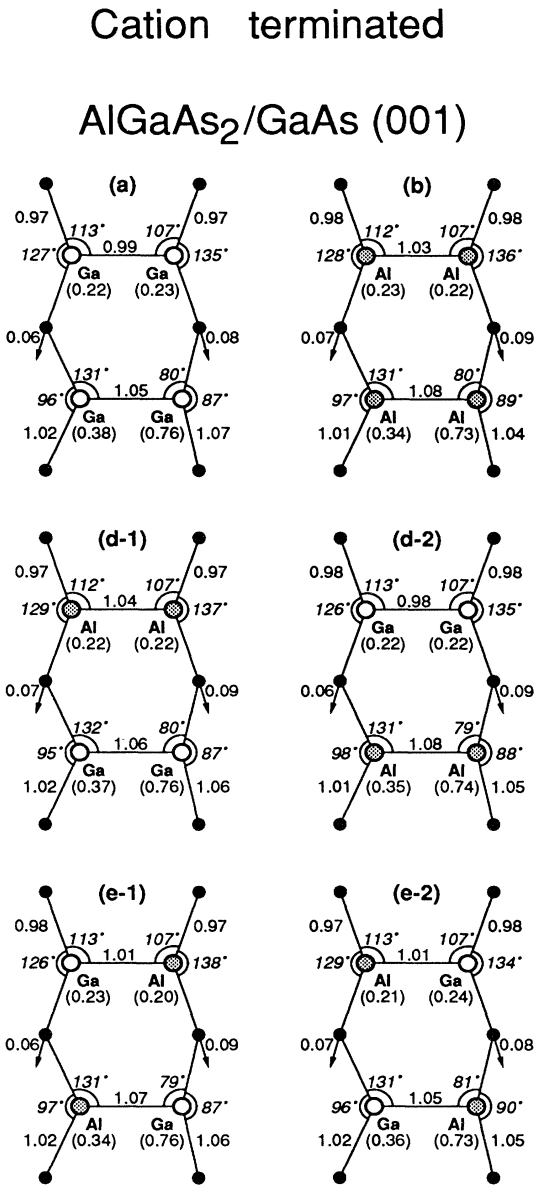

FIG. 7. Schematic top view of the 2×2 unit cell depicting fully relaxed and reconstructed geometries (dimerized, buckled, and tilted) for the *a*, *b*, *d*, and *e* cation-terminated $AlGaAs_2$ prototype surfaces. For the *d* and *e* surfaces we show the two variants with Ga up (1) and Al up (2). The notation and units are as in Fig. 6.

E. Absence of ordering in $Al_{0.5}Ga_{0.5}As/GaAs$ (001)

Since $Al_{0.5}Ga_{0.5}As$ does not order (or orders only weakly) when grown on (001) substrates,[20] it is interesting to compare the energies of the $GaInP_2$ surfaces to those of $AlGaAs_2$. We separately considered Ga and Al as the highest atom on the high dimer (Table III). We find that when the Ga atom is in the up position, the energy is lowest. Recall (Sec. V B) that the high atom accepts electrons from the "low" atoms. Since Ga has a deeper lying *s* orbital energy than Al (the calculated LDA *s* orbital energies for Al, Ga, and In are −7.83, −9.17, and −8.46 eV, respectively) and since the *p* orbital energies are similar, the system prefers to have Ga, not Al, as the high atom. Most importantly, we find that the energy of surface *d* is now only 9 meV per surface atom below that of the *e* surface, so the energy difference is negligible compared to kT_g. Hence, the resulting surface topology is likely to be disordered. This is consistent with experiment,[20] where strong ordering is seen only for growth on the [110] surface. Figure 7 tabulates the resulting geometries for these surfaces. Again the major variation is between the high and low dimers. The Ga dimers have Ga—As bond lengths about 2% longer than the Ga—P bond lengths, but are otherwise remarkably similar to the Ga dimers on the $GaInP_2$ surfaces. The Al—As bond lengths are identical to the Ga—As bond lengths, but the Al-Al dimer length is slightly longer than the Ga—Ga dimer length.

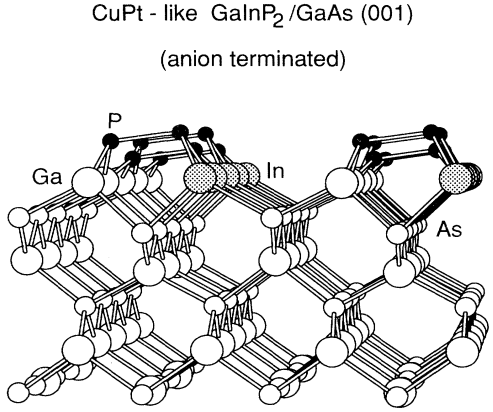

FIG. 8. Side view of the single-surface slab used for the anion-terminated surface calculations. The surface atoms are P (black), Ga (white), and In (grey) on top of a (001) substrate GaAs layer (white).

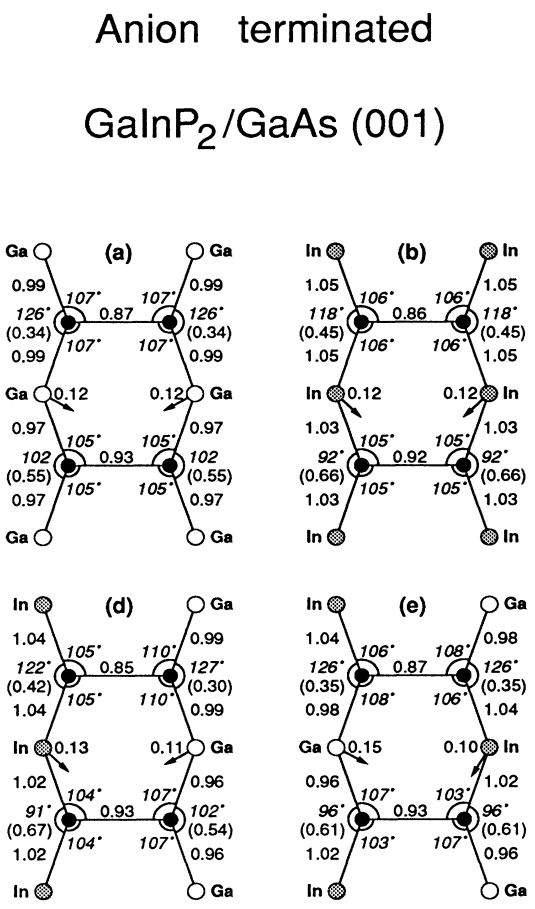

FIG. 9. Schematic top view of the 2×2 unit cell depicting fully relaxed and reconstructed geometries (dimerized, buckled, adn tilted) for the *a*, *b*, *d*, and *e* anion terminated $GaInP_2$ prototpye surfaces. The notation and units are as in Fig. 6.

F. Implications for zinc-blende systems

The buckled and tilted surfaces described above should be considered as a possible candidate geometry for cation-terminated surfaces of binary III-V semiconductors. A 2×4 cell is frequently observed,[55,56] and is believed to be a partially covered, dimerized surface with one out of four dimers missing.[55] It should be noticed, however, that a variation of our buckled surface, with a dimer sequence up-up-down-down, would also result in a 2×4 cell. It is possible, however, that the elastic relaxations in the phosphorus sublayer (see Fig. 6) make this variation energetically unfavorable. Another possible modification would be a translation of every second dimer chain by $a/\sqrt{2}$ along the chain. This would lead to a (4×2) cell with alternating high-low dimers also in the direction perpendicular to the dimer chains. We find that the chain-chain interaction is weak, and that this "chain sliding" modifies the energy by less than 10 meV/surface atom.

VI. PSEUDOPOTENTIAL STUDIES OF THE ANION-TERMINATED SURFACES

We next ask how surface energies are modified when the cation layers are covered by phosphorus. We denote this first subsurface layer by $h=1$. As before, we use a 2×2 unit cell and calculate the energies of the prototype topologies (*a*, *b*, *d* and *e* on a GaAs substrate) but all covered by a single monolayer of P that is allowed to dimerize. The P-P dimer length is found to be shorter than the Ga-In cation dimer length, leading to much larger subsurface relaxations (compare the cation surfaces in Figs. 3 and 4 with the anion surface illustrated in Fig. 8). For this reason we exclusively used a single-surface slab with $7\frac{1}{2}$-monolayer thickness. The resulting dimer geometries are tabulated in Fig. 9. In addition to the dimerization we observe a buckling of the alternate dimers. The buckling is less than that for the cation sur-

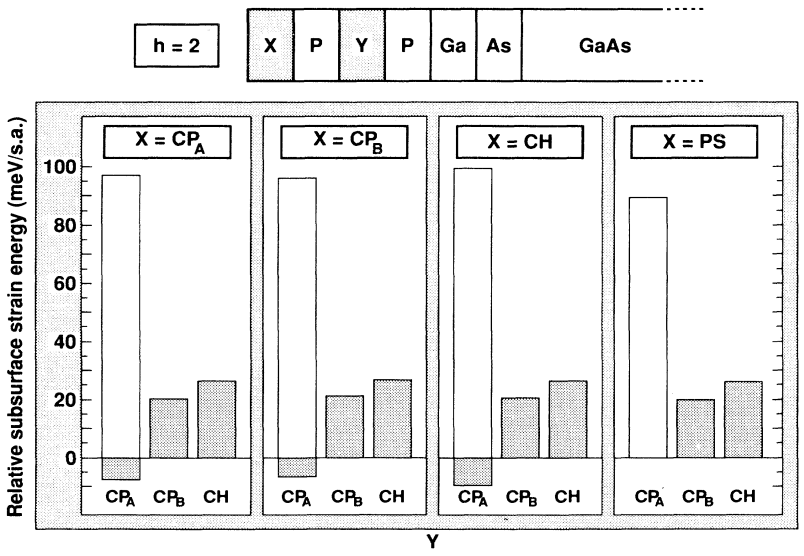

FIG. 10. Strain energies of $GaInP_2$ due to structural changes in the second subsurface layer ($h=2$). Each panel gives the energies of the *c*, *d*, and *e* topologies in layer *Y* (relative to phase separation $a+b$), for specific topologies in layer *X*. The empty and shaded bars correspond to translations of the pattern by $a/\sqrt{2}$ in the [110] or [$\bar{1}$10] directions.

TABLE III. Surface energies for fully reconstructed cation-terminated $Al_{0.5}Ga_{0.5}As/GaAs$ (001) system. The energies are in meV per surface atom relative to the $a+b$ phase-separated surface. The dimer type (Al up or Ga up) refers to the atom farthest from the surface.

Dimer type	Surface type $a+b$	d	e
Al up	0	38	7
Ga up	0	−35	−26

face (compare Figs. 6 and 9), and the dimers are horizontal. The surfaces are still metallic and therefore likely to undergo additional reconstruction. Using arguments similar to those we used for the cation surfaces, a semiconducting surface might possibly be achieved in a 4×2 cell with three high dimers followed by a low. Within the 2×2 cell we find that the e surface has the lowest energy, nearly degenerate with d (3 meV higher) and that the phase-separated $(a+b)$ is 33 meV higher. Thus, the $h=1$ layer affords little structural selectivity.

VII. VALENCE-FORCE-FIELD CALCULATIONS OF BURIED CATION LAYERS

Having discussed the relative energies of the cation-terminated ($h=0$) and anion-terminated ($h=1$) surfaces, we now turn to discussion of the energies of more deeply buried ($h\geq2$) cation layers. Figures 10–13 show the slab structures and results of our VFF calculations of the subsurface strain energies for $h=2$, 3, 4, and 5, respectively, where the hth layer (denoted Y in Figs. 10–13) can have each of the topologies shown in Fig. 2, i.e., $CP_A=c$, $CP_B=d$, and $CH=e$ or phase separated (PS). In each case the top two layers were frozen in the pseudopotential-determined geometry, and their strain energy was omitted. The energies are given relative to the phase-separated state (the average of the pure Ga [Fig. 3(a)] and pure In [Fig. 3(b)] configurations) in the hth layer, since absolute comparisons of the strain energies with different surfaces (denoted X in Figs. 10–13) and/or different values of h are not meaningful on account of omission of surface strain and chemical energies and the chemical-energy difference engendered when transmuting a layer of GaAs into $GaInP_2$ or vice versa. Note that the subsurface elastic effects of the surface reconstruction result in a splitting of the energies of the two phase-reversed partners of a particular topology, and these are depicted separately in Figs. 10–13 by the white and shaded areas. We will refer to these phase-reversed structures as subvariants of CP_A CP_B, or CH (the term "variant" is reserved for the A and B partners of the CP structure). The results shown include all of the pseudopotential-calculated surface geometries (X) discussed above. Layer-by-layer discussion of the results follows.

A. Results for $h=2$

The cation-terminated surfaces should have a mirror-plane symmetry operation located at each dimer (with the mirror plane being vertical and containing the dimer), whereas the pseudopotential-determined geometry exhibits a small breaking of that symmetry caused by the residual interaction between the (mutually rotated) top and bottom surfaces. This symmetry breaking causes a small spurious splitting of the energies of the CP_B and CH subvariants at $h=2$, and to avoid this we have imposed the symmetry on the surface geometries used to generate Fig. 10 (only). The results show that all subsurface cation ar-

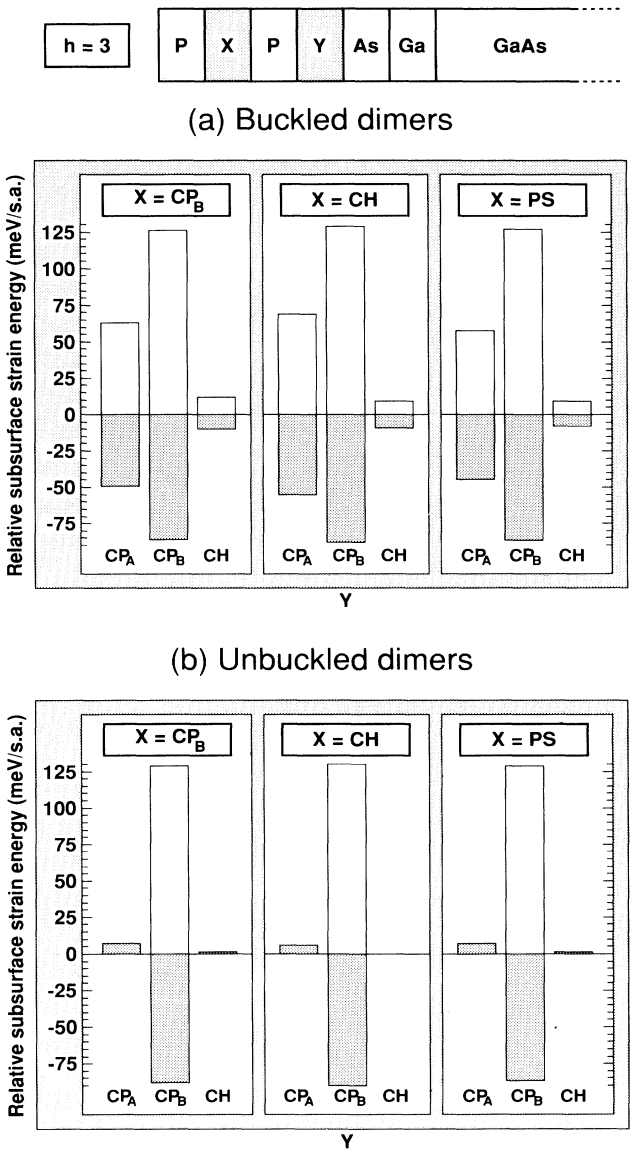

FIG. 11. Strain energies of $GaInP_2$ due to structural changes in the third subsurface layer ($h=3$). Each panel gives the energies of the c, d, and e topologies in layer Y (relative to phase separation $a+b$), for specific topologies in layer X. The empty and shaded bars correspond to translations of the pattern by $a/\sqrt{2}$ in the [110] or [$\bar{1}$10] directions. We show the energies of the layers underneath a P-terminated surface with buckled dimers (a) and with the buckling removed (b).

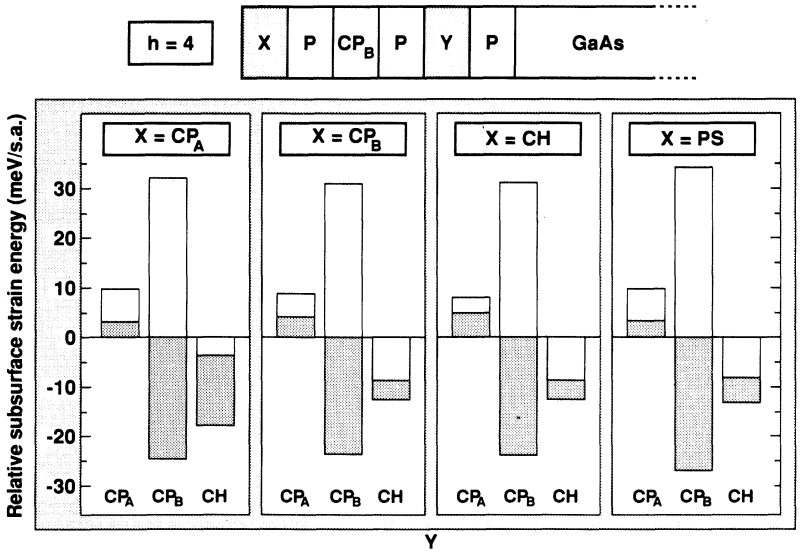

FIG. 12. Strain energies of $GaInP_2$ due to structural changes in the fourth subsurface layer ($h=4$). Each panel gives the energies of the c, d, and e topologies in layer Y (relative to phase separation $a+b$), for a specific topology in layer X. The empty and shaded bars correspond to translations of the topologies by $a/\sqrt{2}$ in the [110] or [$\bar{1}$10] directions.

rangements X have similar energies, except the high-energy CP_A subvariant, whose energy is considerably higher than the others. The low-energy CP_A subvariant is favored slightly (by about 10 meV/surface atom) over the next lowest-energy arrangement, the phase-separated state. Note the very large splitting between the CP_A subvariants induced by the surface reconstruction, and the relatively weak dependence of the relative subsurface strain energies on the topology of the surface (X). The former reflects the strong influence that surface reconstructions exert on subsurface layers, and the latter reflects the strong similarities in the reconstructions of the various cation-terminated surfaces. One can gain a qualitative understanding of the reason CP_A is favored over the other ordered structures and why the two CP_A subvariants exhibit such large splitting by examination of Fig. 14(a), which shows the VFF-relaxed atomic positions for the CP_B surface on a thick GaAs substrate. The arrows indicate the major relaxation directions of subsurface atom rows in response to primarily bond-angle constraints induced by dimerization of surface cations. From these one can see that in the second subsurface layer the [$\bar{1}$10]-oriented row of atoms beneath the surface dimer row has stretched bonds relative to its parallel partner that does not lie beneath a dimer row. Thus, if that layer is occupied by a mixture of Ga and In atoms, the In atoms will prefer to lie beneath the dimer row, and the Ga atoms in the adjacent row, thus producing a layer of the CP_A type. The other CP_A subvariant would have the rows reversed, and would produce the worst possible elastic fit, thereby having much higher strain energy. Hence, dimerization of the cation surface both favors CP_A at $h=2$ and splits the energies of CP_A into two subvariants in that layer.

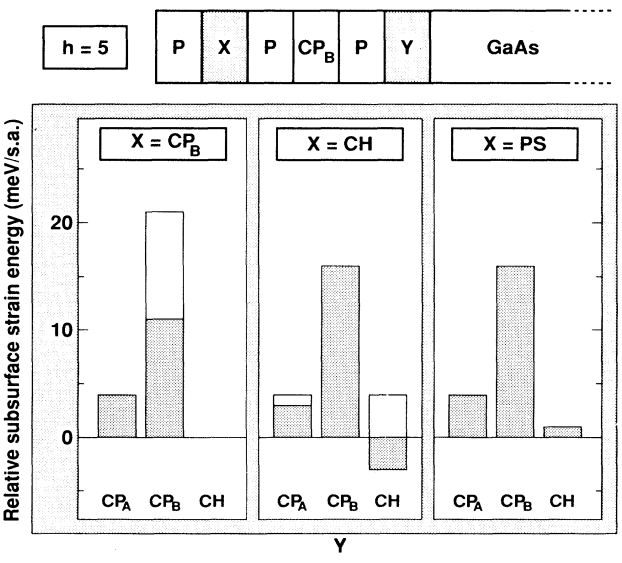

FIG. 13. Strain energies of $GaInP_2$ due to structural changes in the fifth subsurface layer ($h=5$). Each panel gives the energies of the c, d, and e topologies in layer Y (relative to phase separation $a+b$), for a specific topology in layer X. The empty and shaded bars correspond to translations of the pattern by $a/\sqrt{2}$ in the [110] or [$\bar{1}$10] directions.

B. Results for $h=3$

For $h=3$ shown in Fig. 11 (which has an anion-terminated surface) the energy selectivity is much greater, with the CP_B layer structure being preferred by about 35 meV/surface atom over the lowest-energy CP_A subvariant, regardless of the topology of the first subsurface layer (X). Note also the large splitting of the two subvariants of CP_B and those of CP_A. One can understand these trends qualitatively by inspecting Figs. 14(c) and 14(d), which show the first-principles-relaxed atomic positions for the CP_B surface on a GaAs substrate, with arrows indicating major relaxation directions of subsurface atom rows. In Fig. 14(c) we see row relaxations in-

duced primarily by *dimerization* of the surface P atoms. It is clear that at $h=3$ one of the CP_B subvariants provides the best fit, with the other CP_B subvariant providing the worst fit. In Fig. 14(d) we see row relaxations induced primarily by *buckling* of the surface dimer rows, and there it is clear that the two CP_A subvariants provide, respectively, the best and worst fits. That one of the CP_B subvariants wins out overall is a consequence of the larger relaxations induced by dimerization than by buckling.

Because the 2×2 cell used in the first-principles calculations may not permit an accurate representation of the ground-state surface reconstruction of the *anion*-terminated surfaces (e.g., the calculated surfaces are still metallic), we also show in Fig. 11(b) the subsurface strain energies of anion-terminated surfaces with the buckling of the frozen surface removed, i.e., with a (2×1) surface symmetry. In this case the splitting of the CP_A and CH subvariants disappears, as expected. The amount by which the lowest CP_B subvariant is favored over the nearest competitor (now phase separation) is increased to ~90 meV/surface atom, comparable to the energy selectivity at the cation-terminated ($h=0$) surface. This large energy preference for CP_B induced at $h=3$ by the dimerization of the P surface is similar to the mechanism proposed by LeGoues *et al.*[43] to explain one type of ordering observed in SiGe alloys. The quantitative difference in the degree of energy selectivity between $h=2$ (Fig. 10) and $h=3$ (Fig. 11) is primarily a result of the fact that the P-P dimers of the anion-terminated surface are more tightly bound than their cation counterparts, thus inducing greater subsurface strain. Comparison of the $h=3$ results for buckled and unbuckled surfaces [Figs. 11(a) and 11(b), respectively] indicates that splitting of the CP_A and CH variants by higher-order (than mere dimerization) reconstructions can alter the details of the picture somewhat, but the dominant selectivity is due to the dimerization itself, and we expect that the preference for CP_B is likely to survive the smaller degree of buckling likely to be found in a calculation using a larger surface unit cell provided the dimers are organized in chains.

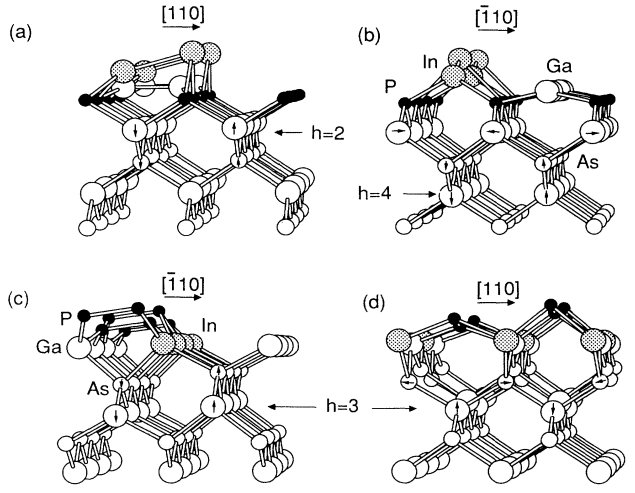

FIG. 14. Side view of atomic geometries for the cation terminated [(a) and (b)] and anion-terminated [(c) and (d)] $GaInP_2$ *d* surfaces. The surface atoms are Ga (white), In (grey), and P (black) on top of a (001) substrate GaAs layer (white). The arrows illustrate the relaxation of subsurface atom rows (see text).

C. Results for $h=4$

For $h=4$ shown in Fig. 12 (which has a cation-terminated surface) we find that the relative energies are only weakly dependent on the topology of the second subsurface layer, so we show only those energies for which that layer has the lowest energy, i.e., the CP_B layer structure. Here again CP_B is favored over the other structures, though the next lowest-energy structure (CH) is only 7–15 meV/surface atom higher in energy, depending on the surface topology. Figure 14(b) shows the major row relaxations, induced primarily by *buckling* of the surface dimer rows. One can see from these that the two CP_B subvariants provide the best and worst fits at $h=4$. We are not certain as to the degree to which the preference for the lowest of the CP_B subvariants over the CH structure would survive the enlargement of the surface unit cell to allow more complex higher-order reconstructions, but in any case, the preference is small enough that it may be largely lost at growth temperatures. We note that the low-energy subvariant corresponds to true three-dimensional CuPt ordering of the surface together with the second and fourth subsurface layers, whereas the high-energy subvariant corresponds to having an antiphase boundary between the second and fourth subsurface layers. In contrast, Boguslawski,[52(a)] who did not consider reconstructed surfaces, found the antiphase boundary to give the lower energy.

D. Results for $h=5$

For $h=5$ shown in Fig. 13 (which has an anion-terminated surface) we again present only results for which the third subsurface (cation) layer has the lowest-energy CP_B layer structure, since there is only weak dependence of the relative energies on the state of order of that layer. Here the stability sequence has nearly reverted to that of the bulk,[10,16] with the phase-separated and CH states being the most stable and CP the least stable. We also find little change in the results when the surface buckling is removed. Of the two CP_B subvariants shown under the CP_B surface, the one with the lower energy (by about 10 meV/surface atom) is the one with an antiphase boundary, whereas the higher-energy variant has the true three-dimensional CuPt structure.

E. Summary of subsurface calculations

In summary, we see that the surface *dimerization,* the most well verified and the most energetically profitable

(Table II) of the surface reconstructions found in the first-principles calculations, induces a strong preference for CP_B layer ordering at $h=3$, and weak preference for CP_A at $h=2$, whereas surface dimer row *buckling* induces a weak preference for CP_B layer ordering at $h=4$. Tilting of surface dimers appears to have no major qualitative effect on subsurface layers, though electron counting arguments suggest that it is closely related to the buckling of dimer rows. A nearly bulklike stability sequence is found by $h=5$. We find that surface *energetics* (not kinetics) explains (i) why GaInP/GaAs does not phase separate, (ii) why the ordering is of the (111) type (not CH or CA), (iii) why the (111) ordering occurs on variant B (not A).

VIII. DISCUSSION AND CONCLUSIONS

Our results show that the CP_B topology has the lowest energy both at the free (cation-terminated) $h=0$ surface and at the third $h=3$ subsurface layer, while past the fourth subsurface layer, the energy order of different topologies approaches that of the bulk crystal. Hence, if atoms could freely move to attain the global minimum energy, we will have a CP_B structure in the near-surface layers, and chalcopyrite inside the epitaxial bulk. As discussed, however, in Sec. IV A, atomic mobility is large near the surface, and is slowed down considerably in deeply buried layers. To see how this could produce long-range ordering through the film, consider the following scenarios:

Scenario (i). Assume that the growing surface has cations exposed for a sufficiently long time so that a locally complete (a few surface unit cells) cation-terminated reconstructed surface can form before subsequent coverage,[72] and that bulk diffusion following subsequent coverage is largely ineffective in rearranging the order established at the surface. Local completion could easily be envisioned to occur, for example, via growth at steps. Then (Table II) the first cation layer grown on the substrate would prefer to order in the CP_B topology (presumably with domains of both subvariants present). When the second cation layer is deposited, and takes the CP_B form, no particular preference for phasing (stacking relationship) between that layer and the buried CP_B layer is expected, so both CP_B subvariants would form with more or less equal probability. When the third cation layer is deposited, the strong preference for true CP_B stacking at $h=4$ (rather than formation of an antiphase boundary), would drive the placement of the *surface* CP_B layer to be appropriate within a given domain to the true three-dimensional CP_B stacking begun there when the second cation layer was deposited. Thus, a mix of domains of the two CP_B subvariants would be formed, with the degree of order depending on the degree of surface CP_B-layer order achieved, as well as on subsequent disordering of buried cation layers through slower bulk diffusion.

Scenario (ii). Assume that the growing surface does not have cations exposed for a sufficient time needed to form CP_B at the surface, and that subsurface diffusion occurs at a substantial rate to a depth of $h=3$ but becomes insignificant thereafter. Then, each mixed-cation layer, as it passes through a depth of $h=3$, would rearrange into a CP_B layer structure (Fig. 11) as a result of the *dimerization* of the P-terminated surface, regardless of the state of order of the mixed-cation layer above it at $h=1$. However, in the absence of significant lifetimes for cation-terminated surfaces, we cannot invoke the CP_B layer-phasing mechanism that occurs at $h=4$ and need to look further for a layer-phasing mechanism that would be active with P-terminated surfaces. At present we know of no such mechanism, though it is possible that surface steps may exert some influence through a choice of which pairs of rows of atoms dimerize or through an enhancement of the probability of formation of CP_B at $h=1$ with fixed phase relative to the CP_B layer at $h=3$. The latter would not require diffusion to $h=3$, but only to $h=1$ (or at steps). Note that ordering was observed to occur only in a "window" of temperatures. It is hence natural to assume in this scenario that if the temperature is too low, then only layers $h=0,1$ are fluid, and ordering does not occur since $h=1$ has but a small ordering selectivity (Sec. VI). On the other hand, if the temperature is too high, even layers 4 and 5 are fluid, and again ordering does not occur, since these layers too have small structural selectivity (Figs. 12 and 13). At intermediate temperatures, where diffusion penetrates to $h=3$ (but no further), ordering is maximized because of the significant energetic preference for CP_B ordering there (Fig. 11).

Scenario (iii). A variation of the scenario above involves the assumption of a locally complete cation-terminated surface existing for a time too short for surface diffusion to create much CP_B ordering at $h=0$, but long enough for the reconstruction of that surface to take place. Assume further that there is a gradual falloff of subsurface diffusion with increasing depth into the film, rather than a relatively abrupt falloff for $h>3$. Then when the only slightly ordered surface is buried to a depth of $h=3$, the CP_B ordering will be enhanced by the (somewhat limited) subsurface diffusion. At this level, the initially small degree of ordering will select a surface P-P dimerization pattern that will, in turn, enhance the existing CP_B order at the expense of the other variant. When this layer passes to $h=4$, it will dictate the pattern of cation-surface reconstruction such that the small degree of CP_B order achieved there will have the correct phase with respect to the $h=4$ layer, so that true three-dimensional CP_B ordering results, though the imperfections due to rapid coverage of the cations at $h=0$ and the limited subsurface diffusion at $h=3$ would be substantial.

All of our results and the foregoing discussion have applied to mixed-cation materials, in particular $GaInP_2$. However, spontaneous ordering into the CuPt structure has been observed in a number of mixed-anion III-V systems as well, and it has been conclusively verified[73] that the structure observed there is also CP_B, rather than CP_A. Some previous hypotheses concerning mechanisms for surface-driven ordering[25] correctly predict CP_B ordering in mixed-cation systems, but erroneously predict CP_A ordering in mixed-anion systems. Our calculations for the P-terminated surface, as well as electron-counting arguments, would suggest a buckled dimer structure, which would tend to favor the CP_A structure at $h=0$.

Based on the relaxations seen in Fig. 14(c), we would expect that CP_B is elastically preferred at $h=2$. Thus, while the preferred state of order of the reconstructed surface cannot be ascertained, we can say that the subsurface strain induced by dimerization would still promote CP_B ordering.

ACKNOWLEDGMENT

This work was supported in part by the Office of Energy Research, Materials Science Division, U.S. Department of Energy, under Grant No. DE-AC02-77-CH00178.

[1]S. M. Sze, *Physics of Semiconductor Devices* (Wiley, New York, 1981).

[2]H. C. Casey and M. B. Panish, *Heterostructure Lasers* (Academic, New York, 1978); M. Jaros, Rep. Prog. Phys. **48**, 1091 (1985).

[3]G. B. Stringfellow, J. Phys. Chem. Solids **34**, 1749 (1973); J. Cryst. Growth **27**, 21 (1974); L. M. Foster and J. F. Woods, J. Electrochem. Soc. **118**, 1175 (1971).

[4]M. B. Panish and M. Ilegems, Prog. Solid State Chem. **7**, 39 (1972); K. J. Bachman, F. A. Thiel, and H. Schreiber, Prog. Cryst. Growth Charact. **2**, 171 (1979).

[5](a) V. T. Bublik and V. N. Leikin, Phys. Status Solidi A **46**, 365 (1978); (b) K. Ishida, T. Nomura, H. Tokunaga, H. Ohtani, and T. Nishizawa, J. Less-Common Met. **155**, 143 (1989); (c) L. M. Foster, J. Electrochem. Soc. **121**, 1662 (1974); (d) K. Onabe, Jpn. J. Appl. Phys. **21**, L323 (1982); (e) K. Ishida, T. Shumiya, T. Nomura, H. Ohtani, and T. Nishizawa, J. Less-Common Met. **142**, 135 (1988).

[6]J. Van Vechten, in *Handbook of Semiconductors,* edited by S. P. Keller (North-Holland, Amsterdam, 1980), Vol. 3, p. 1.

[7]P. A. Fedders and M. W. Muller, J. Phys. Chem. Solids **45**, 685 (1984).

[8]G. P. Srivistava, J. L. Martins, and A. Zunger, Phys. Rev. B **31**, 2561 (1985); **38**, 12 984(E) (1988).

[9]Alloys with positive mixing enthalpies $\Delta H^{(O)}>0$ in the disordered phase, but negative formation enthalpies $\Delta H^{(O)}<0$ in some ordered phases are known, e.g., $CdMg(CO_3)_2$ [C. Capobianco, B. Burton, P. Burton, P. M. Davidson, and A. Navrotsky, J. Solid State Chem. **71**, 214 (1987)] and dolomite $CaMg(CO_3)_2$ [A Navrotsky and C. Capobianco, Am. Mineral. **72**, 782 (1987)].

[10]R. G. Dandrea, J. E. Bernard, S.-H. Wei, and A. Zunger, Phys. Rev. Lett. **64**, 36 (1990).

[11](a) J. L. Martins and A. Zunger, Phys. Rev. Lett. **56**, 1400 (1986); (b) Phys. Rev. B **30**, 6217 (1984); (c) J. Mater. Res. **1**, 573 (1986).

[12]A. A. Mbaye, L. G. Ferreira, and A. Zunger, Phys. Rev. Lett. **58**, 49 (1987); L. G. Ferreira, A. A. Mbaye, and A. Zunger, Phys. Rev. B **35**, 6475 (1987); **37**, 10 547 (1988).

[13]S.-H. Wei and A. Zunger, J. Vac. Sci. Technol. A **6**, 2597 (1988).

[14]J. E. Bernard, L. G. Ferreira, S.-H. Wei, and A. Zunger, Phys. Rev. B **38**, 6338 (1988); J. E. Bernard, R. G. Dandrea, L. G. Ferreira, S. Froyen, S.-H. Wei, and A. Zunger, Appl. Phys. Lett. **56**, 731 (1990).

[15]S.-H. Wei and A. Zunger, Phys. Rev. Lett. **61**, 1505 (1988); R. Magri, S.-H. Wei, and A. Zunger, Phys. Rev. B **43**, 1584 (1991).

[16]L. G. Ferreria, S.-H. Wei, and A. Zunger, Phys. Rev. B **40**, 3197 (1989); S.-H. Wei, L. G. Ferreira, and A. Zunger, *ibid.* **41**, 8240 (1990).

[17]J. E. Bernard and A. Zunger, Phys. Rev. B **44**, 1663 (1991).

[18]There are two distinct rhombohedral superlattice structures for IV-IV systems: the RH1 form, in which the Si-Ge interfaces occur within bilayers along (111) containing one layer each of Si and Ge (intrabilayer or mixed-bilayer interfaces), and the RH2 form, in which the interfaces occur between bilayers (interbilayer or pure-bilayer interfaces). The bilayer sequence in RH1 is (SiGe)(GeSi)$\cdots$, while in RH2 it is (SiSi)(GeGe)$\cdots$. RH1 is a topologically unconstrained structure in that it has zero strain energy when no external constraints are applied. This can be understood geometrically by realizing that the mixed bilayers that constitute the interfaces in RH1 have the Si—Ge bond lengths and angles fully relaxed at the RH1 lattice constant (essentially the average of the Si and Ge lattice constants), and the bilayers are then free to adjust along [111] until both the Si—Si and Ge—Ge bonds joining them are fully relaxed, with *no cost* in bond-angle strain, since these bonds are aligned along [111].

[19]H. Nakayama and H. Fujita [in *GaAs and Related Compounds 1985,* edited by M. Fujimoto, IOP Conf. Proc. No. 79 (Hilger, Bristol, 1986), p. 289] observed ordering in $In_{0.5}Ga_{0.5}As/InP$ (001) grown by liquid-phase epitaxy. The ordered In_3GaAs_4 and $InGa_3As_4$ (201) structures were later reinterpreted to include $InGaAs_2$ in the (201) chalcopyrite form [see T. S. Kuan, W. J. Wang, and E. L. Wilkie, Appl. Phys. Lett. **51**, 51 (1987)].

[20]T. S. Kuan, T. F. Kuech, W. I. Wang, and E. L. Wilkie, Phys. Rev. Lett. **54**, 201 (1985).

[21]Ordering in $GaInP_2$ was discussed by A. Gomyo, T. Suzuki, and S. Iijima, Phys. Rev. Lett. **60**, 2645 (1988); A. Gomyo, K. Kobayashi, S. Kawata, I. Hino, and T. Suzuki, J. Crys. Growth **77**, 367 (1986); A. Gomyo, T. Suzuki, K. Kobayashi, S. Kawata, I. Hino, and T. Kusas, Appl. Phys. Lett. **50**, 673 (1987).

[22]The effect of substrate orientation on ordering in $GaInP_2$ was discussed by A. Gomyo, T. Suzuki, S. Iijima, H. Hotta, H. Fujii, S. Kawata, K. Kobayshi, Y. Ueno, and I. Hino, Jpn. J. Appl. Phys. **27**, L2370 (1988); A. Gomyo, S. Kawatawa, T. Suzuki, S. Iijima, and I. Hino, *ibid.* **28**, L1728 (1989); T. Suzuki, A. Gomyo, and S. Iijima, J. Cryst. Growth **99**, 69 (1990).

[23]The effect of *p* doping on ordering in $GaInP_2$ was discussed by T. Suzuki, A. Gomyo, I. Hino, K. Kobayashi, S. Kawata, and S. Iijima, Jpn. J. Appl. Phys. **27**, L1549 (1988); F. P. Dabkowski, P. Gavrilovic, K. Meehan, W. Stutius, J. E. Williams, M. A. Shahid, and S. Mahajan, Appl. Phys. Lett. **52**, 2142 (1988); S. R. Kurtz, J. M. Olson, J. P. Goral, A. Kibbler, and E. Beck, J. Electron. Mater. **19**, 825 (1990).

[24]Ordering-induced changes in the band gap of $GaInP_2$ were discussed by T. Suzuki, A. Gomyo, S. Iijima, K. Kobayashi, S. Kawata, I. Hino, and T. Yuasa, Jpn. J. Appl. Phys. **27**, 2098 (1988); Y. Inone, T. Nishino, Y. Hamakawa, M. Kondow, and S. Minagawa, Optoelectron. Dev. Technol. **3**, 61 (1988); T. Nishino, Y. Inone, Y. Hamakawa, M. Kondow, and S. Minagawa, Appl. Phys. Lett. **53**, 583 (1988); S. R. Kurtz, J.

M. Olson, and A. Kibbler, Solar Cells **24**, 307 (1988); Appl. Phys. Lett. **54**, 718 (1989); **57**, 1922 (1990).

[25]T. Suzuki, A. Gomyo, and S. Iijima, J. Cryst. Growth **93**, 396 (1988).

[26]Ordering in $Ga_{0.7}In_{0.3}P$ was discussed by M. Kondow, H. Kakibayashi, T. Tanaka, and S. Minagawa, Phys. Rev. Lett. **63**, 884 (1989).

[27]Influence of growth temperature on ordering in $GaInP_2$ was discussed by M. Kondow, H. Kakibayashi, S. Minagawa, Y. Inone, T. Nishino, and Y. Hamakawa, Appl. Phys. Lett. **53**, 2053 (1988); M. Kondow, H. Kakibayashi, and S. Minagawa, J. Cryst. Growth **88**, 291 (1988); M. Kondow, S. Minagawa, Y. Inone, T. Nishino, and Y. Hamakawa, Appl. Phys. Lett. **54**, 1760 (1989).

[28]Work at Fujitsu Laboratories on $GaInP_2$ ordering includes S. Ueda, M. Takikawa, J. Komeno, and I. Umebu, Jpn. J. Appl. Phys. **26**, L1824 (1987); O. Ueda, M. Takikawa, M. Takechi, J. Komeno, and I. Umebu, J. Cryst. Growth **93**, 418 (1988); O. Ueda, M. Takechi, and J. Komeno, Appl. Phys. Lett. **54**, 2312 (1989); O. Ueda, M. Hoshino, K. Kodama, H. Yamada, and M.Ozeki, J. Cryst. Growth **99**, 560 (1990); H. Okuda, C. Anayama, S. Narita, M. Kondo, T. Tanahashi, O. Ueda, and K. Nakejima, Appl. Phys. Lett. **55**, 690 (1989).

[29]Models of substrate-induced ordering in $GaInP_2$ were advanced by P. Bellon, J. P. Chevalier, L. Augarde, J. P. André, and G. P. Martin, J. Appl. Phys. **66**, 2388 (1989).

[30]S. McKernan, B. C. DeCooman, C. B. Carter, D. P. Bour, and J. R. Shealy, J. Mater. Res. **3**, 406 (1988).

[31]CH and CA ordering in $InGaAs_2$ was discussed in Ref. 15.

[32]CH and CA ordering in Ga_2AsSb/InP (001) was seen by H. R. Jen, M. J. Cherng, and G. B. Stringfellow, J. Appl. Phys. **48**, 1603 (1986); H. R. Jen, M. J. Cherng, M. J. Jou, and G. B. Stringfellow, in *GaAs and Related Compounds, 1986,* edited by W. T. Lindley, IOP Conf. Ser. Proc. No. 83 (Institute of Physics, Bristol, 1987), p. 159; H. R. Jen, M. J. Jou, Y. T. Cherng, and G. B. Stringfellow, J. Cryst. Growth. **85**, 175 (1987).

[33]CP ordering in Ga_2AsSb/InP (001) has been seen in OMVPE growth by G. B. Stringfellow, J. Cryst. Growth **98**, 108 (1989); J. J. Murgatroyd, A. G. Norman, and G. R. Booker, J. Appl. Phys. **67**, 2310 (1990); A. G. Norman, R. E. Mallard, I. J. Murgatroyd, G. R. Booker, A. H. Moore, and M. D. Scott, in *Microscopy of Semiconducting Materials,* edited by A. G. Cullis and P. D. Augustus, IOP Conf. Proc. No. 87 (Institute of Physics, Bristol, 1987), p. 77; Y. E. Ihm, N. Otsuka, J. Klem, and H. Morkoc, Appl. Phys. Lett. **51**, 2013 (1987); N. Otsuka, Y. E. Ihm, Y. Hirotsu, J. Klem, and H. Morkoc, J. Cryst. Growth **95**, 43 (1989).

[34]CP ordering was seen in $In_2AsSb/InSb$ (001) by H. R. Jen, K. Y. Ma, and G. B. Stringfellow, Appl. Phys. Lett. **54**, 1154 (1989).

[35]CP ordering was seen in $AlInP_2/GaAs$ (001) by M. Kondow, H. Kakibayashi, and S. Minagawa, Phys. Rev. B **40**, 1159 (1989).

[36]CP ordering and phase separation were seen in $GaInAs_2/InP$ (001) and GaInAsP by M. A. Shahid, S. Mahajan, D. E. Laughlin, and H. M. Cox, Phys. Rev. Lett. **58**, 2567 (1987); M. A. Shahid and S. Mahagan, Phys. Rev. B **38**, 1344 (1988); T. L. McDevitt, S. Mahajan, D. E. Laughlin, W. A. Bonner, and V. G. Keramidas, in *Epitaxial Heterostructures,* edited by D. W. Shaw, J. C. Bean, V. G. Keramidas, and P. S. Peercy (Material Research Society, Pittsburgh, 1990), Vol. 198, p. 609.

[37]CP ordering was seen in $InAlAs_2/InP$ (001) by O. Ueda, T. Fujii, Y. Nakada, H. Yamada, and I. Umebu, J. Cryst. Growth **95**, 38 (1989).

[38]CP ordering was seen in Ga_2AsP grown (001) on an alloy substrate by H. R. Jen, D. S. Cao, and G. B. Stringfellow, Appl. Phys. Lett. **54** 1890 (1989); W. E. Plano, D. W. Nam, J. S. Major, K. C. Hsieh, and N. Holonyak, *ibid.* **53**, 2537 (1988).

[39]CP ordering was seen in AlGaInP/GaAs (001) by H. Okuda, C. Anayama, T. Tanahashi, and K. Nakejima, Appl. Phys. Lett. **55**, 2190 (1989).

[40]A. Ourmazd and J. C. Bean, Phys. Rev. Lett. **55**, 765 (1985).

[41]D. J. Lockwood, K. Rajan, E. W. Fenton, J.-M. Baribeau, and M. W. Denhoff, Solid State Commun. **61**, 465 (1987).

[42]E. Müller, H.-U. Nissen, M. Ospelt, and H. von Känel, Phys. Rev. Lett. **63**, 1819 (1989).

[43]F. K. LeGoues, V. P. Kesan, and S. S. Iyer, Phys. Rev. Lett. **64**, 40 (1990); F. K. LeGoues, V. P. Kesan, S. S. Iyer, J. Tersoff, and R. Tromp, *ibid.* **64**, 2038 (1990).

[44]W. I. Wang [J. Appl. Phys. **58**, 3244 (1985)] suggested that charge transfer between As and Ga would set up a Madelung energy that would stabilize the CuAu-like structure, and hence explain the observed ordering. However, D. M. Wood, S.-H. Wei, and A. Zunger [Phys. Rev. B **36**, 1342 (1988), Eqs. (23) and (25)] showed that the relevant quantity in such an electrostatic model is the *excess* Madelung energy of a given structure with respect to that of the constituents. This, hence, depends both on the difference $\Delta q = q_A - q_B$ between the A charge in AC and B charge in BC, and the differnce $\Delta Q = Q_A - Q_B$ between the A and B charges in the CuAu structure. For the *excess* Madelung energy to be negative, one needs that $\Delta Q/\Delta q > 1.83$, a situation not supported for $AlGaAs_2$ by any first-principles calculation.

[45]M. Van Schilfgaarde, A. B. Chen, and A. Sher [Phys. Rev. Lett. **57**, 1149 (1986)] considered the excess Coulomb energy of various lattices, including both intersite (Madelung) and on-site Coulomb terms. They concluded that these terms may account for the observed ordering in $Al_{1-x}Ga_xAs$. However, S.-H. Wei [*ibid.* **59**, 2613 (1987)] found a (double-counting) error of a factor of 2 in one of their terms; correcting this error showed that Coulomb effects do not distinguish the excess electrostatic energies of the random alloy from the phase-separated or the CuAu-ordered structure.

[46]J. S. Cohen and A. G. Schlijper [Phys. Rev. B **36**, 1526 (1987)] calculated the excess energies of ordered $Ga_nAl_{4-n}As_4$ structures using the augmented spherical wave (ASW) method, finding $\Delta H^{(CA)} < 0$. An error in treating inequivalent atomic spheres as equivalent, corrected by them later [**38**, 12 694 (1988)] showed, however, that $\Delta H^{(CA)} > 0$ for this structure.

[47]B. Koiller, M. A. M. Davidovich, and L. M. Falicov [Phys. Rev. B **41**, 3670 (1990)] calculated the electronic excess energies of 16 ordered structures of $Al_nGa_mAs_{n+m}$ using the empirical tight-binding method, finding that among these, the CuAu-I-like structure has the lowest energy. R. Magri and A. Zunger [*ibid.* **43**, 1584 (1991)] pointed out that the use of a single **k** point (the center of the supercell Brillouin zone) in this calculation led to significant numerical errors. Correcting these then leads to $\Delta H^{(CA)}_{bulk} > 0$.

[48]Y. T. Shen, D. M. Bylander, and L. Kleinman [Phys. Rev. B **38**, 13 257 (1988)] showed on the basis of a pseudopotential perturbation calculation that the *random* $Al_{0.5}Ga_{0.5}As$ alloy has $\Delta H^{(D)} < 0$ despite $\Delta H^{(CA)} > 0$. They later corrected an error in their calculation [S. Lee, D. M. Bylander, and L. Kleinman, *ibid.* **40**, 8399 (1989)], revealing that $\Delta H^{(CA)} > \Delta H^{(D)} > 0$.

[49]A. A. Mbaye, D. M. Wood, and A. Zunger, Phys. Rev. B **37**,

3008 (1988); D. M. Wood and A Zunger, Phys. Rev. Lett. **61**, 1501 (1988); Phys. Rev. B **38**, 12 756 (1988).

[50]Coherent epitaxial solid solutions of $GaP_{1-x}Sb_x$ on GaAs and GaSb were grown by M. J. Jou, Y. T. Cherng, H. R. Jen, and G. B. Stringfellow, Appl. Phys. Lett. **52**, 549 (1988), GaP and GaSb are mutually insoluable in bulk form.

[51]S. C. Wu, S. H. Lu, Z. Q. Wang, C. K. C. Lok, J. Quinn, Y. S. Li, D. Tian, and F. Jona, Phys. Rev. B **38**, 5363 (1988); E. G. McRae and R. A. Malic, Surf. Sci. **177**, 53 (1986); R. J. Baird, D. F. Ogletree, M. A. Van Hove, and G. A. Somorjai, *ibid.* **165**, 345 (1986).

[52](a) P. Boguslawski, Phys. Rev. B **42**, 3737 (1990); (b) S. Matsumura, N. Kuwano, and K. Oki, Jpn. J. Appl. Phys. **29**, 688 (1990).

[53]T. Kurimoto and N. Hamada, in *Proceedings of the 20th International Conference on Physics of Semiconductors, Thessaloniki, 1990,* edited by E. M. Anastassakis, and J. D. Joannopoulos (World Scientific, Singapore, 1990), p. 300.

[54]P. N. Keating, Phys. Rev. **145**, 637 (1966).

[55]D. K. Biegelsen, R. D. Bringans, J. E. Northrup, and L. E. Swartz, Phys. Rev. B **41**, 5701 (1990).

[56]G. X. Qian, R. M. Martin, and D. J. Chadi, Phys. Rev. B **38**, 7649 (1988).

[57]P. C. Kelires and J. Tersoff, Phys. Rev. Lett. **63**, 1164 (1989).

[58]A. Madhukar and S. V. Ghaisas, CRC Crit. Rev. Solid State Mater. Sci. **14**, 1 (1988).

[59]S. B. Ogale, M. Thomsen, and A. Madhukar, in *Initial Stages of Epitaxial Growth,* edited by R. Hull, J. M. Gibson, and D. A. Smith, MRS Symposia Proceedings No. 94 (Materials Research Society, Pittsburgh, 1987), p. 83.

[60]M. Schneider, I. K. Schuller, and A. Rahman, Phys. Rev. B **36**, 1340 (1987); S. M. Paik and S. Das Sarma, *ibid.* **39**, 1224 (1989).

[61]F. Abraham and G. M. White, J. Appl. Phys. **41**, 1841 (1970); G. J. Gilmer, J. Cryst. Growth **49**, 465 (1980).

[62]P. M. Petroff, J. M. Gaines, M. Tsuchiya, R. Simes, L. Coldren, H. Kromer, J. English, and A. C. Gossard, J. Cryst. Growth **95**, 260 (1989).

[63]J. Ihm, A. Zunger, and M. L. Cohen, J. Phys. C **12**, 4409 (1979).

[64]We used a checkerboard 2×2 vacancy pattern instead of the 2×1 pattern used by D. J. Chadi [J. Vac. Sci. Technol. A **5**, 834 (1987)].

[65]J. P. Perdew and A. Zunger, Phys. Rev. B **23**, 5048 (1981).

[66]D. Vanderbilt, Phys. Rev. B **32**, 8412 (1985).

[67]S. Froyen, Phys. Rev. B **39**, 3168 (1988). We use the generating vectors $f_0=2\pi/a$ $(\frac{1}{8},\frac{1}{8},0)$, $f_1=2\pi/a$ $(\frac{1}{4},0,0)$, $f_2=2\pi/a$ $(0,\frac{1}{4},0)$, and $f_3=2\pi/c$ (0,0,1), where a is the alloy lattice constant and c is the thickness of the slab plus vacuum.

[68]J. L. Martins and A. Zunger, Phys. Rev. B **30**, 6217 (1984).

[69]W. H. Press, B. P. Flannery, S. A. Teukolsky, and W. T. Vetterling, *Numerical Recipes* (Cambridge University, Cambridge, 1986), pp. 301–306.

[70]The heteropolar dimers on the c and e surfaces were allowed to tilt naturally.

[71]For the e surface, we allowed asymmetric dimers and found a local, possibly metastable energy minimum with slightly tilted dimers. For the c surface we were unable to find such a local minimum.

[72]It is not obvious that the total energy of a $\Theta=1$ monolayer of cation coverage in the alloy is lower than that of a "missing dimer" $\Theta=\frac{3}{4}$ monolayer, where the remaining cation is in a metallic form. In pure GaAs, the $\Theta=\frac{3}{4}$ *is* more stable than $\Theta=1$.

[73]G. S. Chen, D. H. Jaw, and G. B. Stringfellow, J. Appl. Phys. **69**, 4263 (1991).